UNIVERSITÀ POLITECNICA DELLE MARCHE
FACOLTÀ DI INGEGNERIA

Corso di Laurea Magistrale in Biomedical Engineering

Estimation of Continuous Joints Angles during Gait from Myoelectric Signal

Relatore:
Prof. Federica Verdini

Tesi di Laurea di:
Valeria Scolastra

Correlatori:
Prof. Sandro Fioretti
Ing. Andrea Tigrini

A.A. 2021/2022

Acknowledgments

For the development of this thesis, I would like to thank my Supervisor Federica Verdini, co-Supervisors Sandro Fioretti and Andrea Tigrini, and Alessandro Mengarelli for the precious indications and the constant support shown me in recent months, for helping me during my internship and for reviewing the present manuscript. I would like to strongly thank my fellow student Federica Cerritelli, who shared with me this important moment of our university careers. Special thanks to my family and friends, for supporting me over these years.

Contents

ABSTRACT

Introduction. This thesis aims to propose a robust and reliable method for the estimation of continuous joints angles during the task of ground level walking from myoelectric signals. We aim to provide an approach able to estimate ankle, knee, and hip angles from larger amount of data. Regression is performed firstly on each trial, then inter-trial regression approach is done on the same subject. We aim to verify which of the models considered of Neural Network regression can provide a robust estimation of continuous joints angles by taking into account different amount of training and testing data. We start from a model with large amount of training data with respect to testing data, to arrive to a model with a reduced set of data for the training with respect to testing data. Another important aim of this study is to verify which of the main superficial leg muscles can provide a robust estimation of continuous joints angles respect to others once the validity of the regression model is confirmed by all electrodes' setup configuration. In particular, the aim is to analyze what happens to regression performance if one considers proximal muscles respect to distal muscles and to verify the effectiveness of the model by reducing the muscles from the initial electrode' setup.

Materials and methods. 6 healthy subjects are asked to walk on the Laboratory's platform for about 3 minutes (that corresponds to about 70 steps). EMG signals are acquired by 6 electrodes positioned on the right leg of each subject, 3 on the shank and 3 on the thigh. Ankle, knee, and hip angles are obtained according to the Davis protocol. Once the signals are processed and EMG signals segmented, 4 features are extracted to constitute one feature set (see Section 2.6.2): Mean Absolute Value (MAV), Root Mean Square (RMS), Waveform Length (WL) and Integrated Absolute Value (IAV). This feature set is used to train and validate models coming from Feed-Forward Neural Network regression architecture. 6 models are built to perform regression of joints angles on each trial for each muscle or group of muscles considered and 2 models are built for inter-trial regression for each group of muscles. Regression performance metrics (RMSE and R^2) are calculated to access the degree of regression accuracy for all regression models. Finally, the Wilcoxon rank sum test is used to evaluate the statistical differences on R^2 metric between the considered models.

Results and discussion. Results obtained in this study reveal that, feed-forward Neural Network models can be used for the estimation of ankle, knee, and hip angles, with best results achieved considering all the electrodes' setup. None of the considered models demonstrates to be statistically different, with exceptions for those used for the hip angle regression on each trial and for the two models employed to regress the ankle angle in the inter-trial regression (in both cases, the models

were defined considering all the six muscles from the initial configuration). For the ankle regression, choosing only the electrodes of the thigh, good results can be achieved with RMSE lower than 6°. If proximal muscles are considered instead, results comparable to all electrodes' setup are achieved. For the knee regression, results proved that the tibialis anterior muscle does not provide reliable estimation supporting the lack of functional role of this muscle for this joint. For the hip regression, just the configuration with all muscles involved gave the best performance (RMSE lower than 4° and R^2 that reaches 0.90).

1 INTRODUCTION

Gait is the way that animals, including humans, move their lower limbs when they are moving over a surface, and it is one of the most fundamental activities [1]. Gait is characterized by a pattern of cyclical motor activity of the inferior limbs and of the trunk that allows to support the body weight on the supported limb and to advance the contralateral limb forward [2]. Recent studies have classified gait with preferred definitions based on mechanics [2]–[4]. In fact, gait is also referred to 'gait cycle' or 'cycle time' and it is usually considered one cycle time as the time interval between two successive occurrences of one of the repetitive events of walking that will be described properly in Section 2.1. The movement of walking requires the body to solve a problem of dynamic balance at all times, where the nervous and musculo-skeletal systems should integrate perfectly. Any alteration in these systems, due to age or pathology, leads to a functional limitation that can be detected and quantified with instrumental techniques and using mathematical models [2].

The analysis of the gait can assist in the diagnosis of diseases that affect one of the involved systems (nervous, musculoskeletal), revealing the degree of functional impairment required for the pathology, facilitating the planning of particular treatments, and providing important elements for assessing the efficacy of rehabilitation interventions [5]. Thus, the study of human locomotion is of great importance. Gait analysis is the systematic study of human motion, using equipment for observing movements, body mechanics, and muscle activity. It is frequently employed in sports biomechanics to assist athletes in running more effectively and to spot posture- or movement-related issues in patients with injuries [6].

Joint angles measurements can be a useful tool for understanding movement in scenarios from simple gym exercises up to complex actions in a wide variety of sports and activities. Joint angle is also often measured in conjunction with other signals, such as EMG, to get even more information about movement or reflexes. Surface EMG signal is the recording of muscle electrical activity and by performing a signal processing procedure on the raw surface EMG signals, muscle activity and body movement information can be obtained. In particular, because of the structural characteristics of the musculoskeletal system, activity levels during human muscle motion are conditioned to generate a significant difference depending on the joint angle [7]. The magnitude of the change or the length of the muscles at the joint location have a significant effect on the maximum power generated by the muscle during the isometric contraction of the element that acts as the length, and the angle of the joint determines the maximum strength of the muscle [8], [9]. Due to its ability to precede changes

in motion, surface EMG is widely studied as a peripheral sensing modality for capturing features of muscle activity as an input for control of powered assistive devices [10].

1.1 State of the art

Many studies in the last decades have focused on the exploitation of surface EMG signals for the estimation of continuous lower-limb movements. Various tasks investigated relies on the importance of human locomotion and on the estimation of joints angles for limb prostheses [11]–[13]. To estimate human joints angles, regression algorithms were employed, involving both machine-learning approaches and neural network-based analysis. A study by Xiong et al. [14] focuses on the estimation of continuous ankle and knee angles, by tracking human gait using surface EMG. Six estimation methods were compared and all of them regard machine-learning approaches: Multi-Layer Perceptron (MLP) Regressor, Polynomial Regressor, Decision Tree Regressor, K-Nearest Neighbors Regressor, Support Vector Regressor and Random Forest Regressor. It was showed that machine learning algorithms are good methods to predict lower limbs joints angles, with knee joint having larger error compared to ankle joint. Attention is devoted also on the specific leg muscles recorded by surface EMG electrodes and used for the estimation of joints angles as well as the features being extracted from EMG signals. In fact, in [14] 7 leg muscles were considered for the analysis, with time-domain features sets widely used due to their low computational complexity but with the compromise of limited information about the data. Models that estimate ankle angle or related moment during more than one condition (e.g., different walking speeds) have been recently described in literature. Further studies evaluate neural network-based approaches for the estimation of joints angles, as the study done by Zabre-Gonzalez et al. [15] and Chen et al. [16]. The letter used a deep belief network and principal component analysis, for EMG dimensionality reduction from ten muscle signals, individually combined with a nonlinear back-propagation network to estimate hip, knee, and ankle angle of healthy participants. Zabre-Gonzalez et al. [21] confirmed the accuracy of neural network regression methods, which show the merit to be simple and quick for the estimation of ankle dorsi-plantar flexion as can be found also in [17]. Most approaches characterize performances during walking on specific terrain (e.g., level walking) as the study of Prasertsakul and Poonsiri [18]. They suggest a regression model based on artificial neural network methods to predict knee and ankle angles during walking defining the relationship between the EMG of 8 muscles and angular displacements of both knee and ankle joints of both legs [18]. The results show that, once again, the neural network regression method is the best with performance of testing set very close to the training set. The main focus of these studies is to provide reliable information for the development of control architectures for active prostheses/orthoses, with sensor inputs used to recognize the user's locomotive intention and generate corresponding control commands able to produce the desired limb movement [19]. Such intelligent prosthetic/orthotic devices are expected to understand the user's

intention using sensor input and assist in performing the required task to replace the lost functionality. An EMG-driven nonlinear autoregressive neural network with exogenous inputs (NARX) with predictive future states can address these challenges and provide a robust and intuitive control of active powered ankle-foot prostheses [20]. Previous works demonstrated the ability of a single-output feedforward (open-loop) NARX model to continuously predict ankle angle of the prosthesis using within-socket EMG activity from the residual limb of transtibial amputees [20], [21]. In the study of Huang et al. [22] an algorithm based on neuromuscular-mechanical fusion was proposed to continuously recognize a variety of locomotion modes performed by patients with transfemoral amputations using Support Vector Machine and recording EMG from gluteal and residual thigh muscles.

1.2 Aim of the study

The main goal of this research is to propose a robust and reliable method for the estimation of continuous joints angles from surface EMG signal during the task of ground level walking. The information extracted from the EMG signal can be exploited to help the patient with a real-time aid for walking. The aim of this study is to provide a solid regression approach to estimate continuously hip, knee and ankle angles during normal ground level walking. Particular attention was devoted to the proper electrodes' setup on the patient's leg, that was done according to recent studies [14], [16]. It is of interest to investigate which of the main superficial leg muscles can provide robust estimation of joints angles respect to others. We considered both specific muscles of one joint, and non-specific muscles (the aim is also to verify the accuracy of the models if the anatomical-functional conditions are not adequate, simulating the case of trans-femoral amputees and thus considering only the muscles of the thigh for the ankle and knee angles regression). Another important aim of this study is the estimation of joints angles by considering different amount of data between training set and testing set, starting from a trained model with more training data with respect to testing data to a trained model with less training data with respect to testing data and evaluate which of the considered model gives the best results. Finally, we aim to verify the accuracy of the model considering as training set and testing set one or more trials of the same subject. In this way, longer training and testing times will be considered, compared to recent studies which instead considered shorter test times or a single cycle time [23], [24]. The following 4 macro-sections of this thesis are Materials and methods (chapter 2) that describes in detail the setup, the walking task, the signal processing phase, the extraction of features and the regression phase. An introduction to gait analysis, with a brief description of the Davis protocol, and a general overview of the main superficial muscles of the lower limb is added. Results (chapter 3) is the section dedicated to all the results that we have carried out from experiments while in Discussion and Conclusion (chapter 4), the results are thoroughly explained and discussed. Moreover, further possible enhancements in estimation of continuous joints angles from EMG signal during gait are proposed.

2 MATERIALS AND METHODS

Starting from the definition and description of the various phases that characterize the gait cycle, a brief overview of gait analysis and the Davis protocol is given as well as an introduction to the main superficial muscles of the lower limb and EMG signal acquisition and processing. Hardware and set up of this study are explained, and it is also given a general description of Neural Network architecture used for the regression. Six models of Neural Network regression were used on each of the trials performed by the subjects, together with two models for inter-trial analysis for each muscle or group of muscles considered from the initial configuration with all muscles in the setup. Finally, once the feature set is presented, the two main regressor performance metrics are explained: RMSE (Root Mean Squared Error) and R^2 (Coefficient of Determination, usually called "R squared").

2.1 Definition of gait cycle

The gait cycle is defined as the time interval between two successive occurrences of one of the repetitive events of walking. It is generally convenient to consider the instant at which one foot contacts the ground (called 'initial contact', that is the phase in which the heel strikes the ground). In this study a series of consecutives strides (a single stride is the distance between two successive heel contacts events for the same h foot) each defined by two heel strikes events are examined. In Figure 1 there are displayed ankle, knee, and hip angles among one cycle time. The major events of one gait cycle referred to one leg are: Initial Contact (IC), Opposite Toe off (OT), Heel Rise (HR), Opposite Initial contact (OI), Toe Off (TO), Feet Adjacent (FA) and Tibia Vertical (TV). These seven events subdivide the gait cycle into seven periods or subphases, four of which occur in the stance phase (Loading response, Mid-stance, Terminal stance and Pre-swing) and three in the swing phase (Initial swing, Mid-swing and Terminal swing) [3], [25].

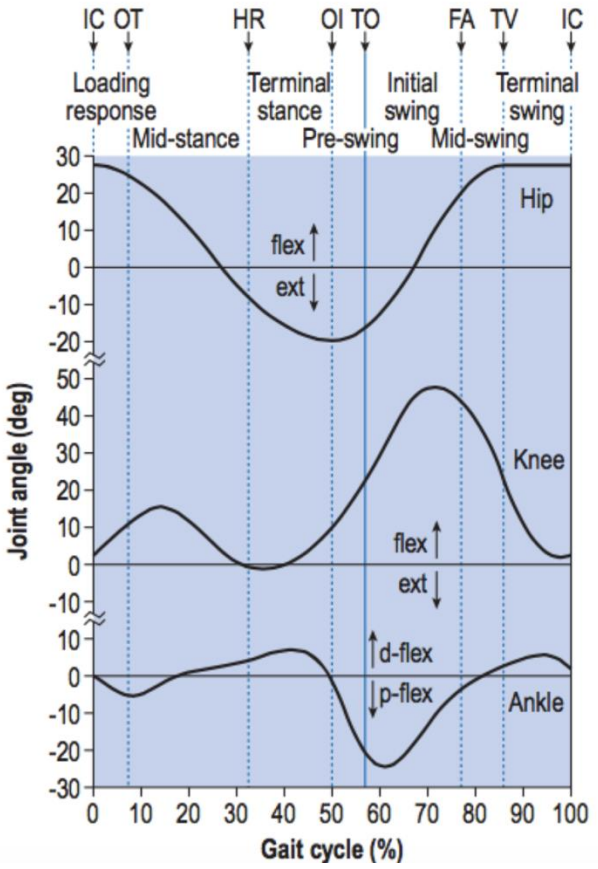

Figure 1: Ankle, knee and hip angles among one cycle time. The stance phase (that starts from IC to TO) constitutes the 60% of the total gait cycle, while the swing phase (from TO to the next IC) the remaining 40%.

In Figure 1 it can be seen that, during a single gait cycle, the hip flexes and extends once. The limit of flexion is reached around the middle of the swing phase and the hip is then kept flexed until initial contact. The peak extension is reached before the end of the stance phase, after which the hip begins to flex again. The knee shows two flexion and two extension peaks during each gait cycle. It is fully extended before IC, flexes during the loading response and the early part of mid-stance, then extends again during the latter part of mid-stance. It starts then flexing again, reaching a peak during initial swing. It extends again prior to IC. The ankle is usually within a few degrees of the neural position for dorsiflexion/plantarflexion at the time of IC. After IC, the ankle plantarflexes, bringing the forefoot down onto the ground. During mid-stance, the tibia moves toward over the foot, and the ankle joint becomes dorsiflexed. Before OI, the ankle angle again changes, and a major plantarflexion takes place until just after TO. In the next Section, there will be described gait analysis with the chosen protocol to obtain ankle, knee, and hip angles, as well as the conventions used to specify joints angles.

2.2 Gait analysis and the Davis protocol

Gait analysis is a methodology to study human locomotion in order to assess the functionality of the neuro-musculoskeletal system, for instance, and through the use of instrumentations it guarantees body movements measurements body mechanics, together with the activity of the muscles [6].
It is also convenient to refer joints angles to precise reference coordinates systems. Positions, displacements, and angles are projected onto a system of planes referred to a person in an upright position [3]. The motion of the limbs is described using reference planes: sagittal plane, frontal plane, and transverse plane (Figure 2).

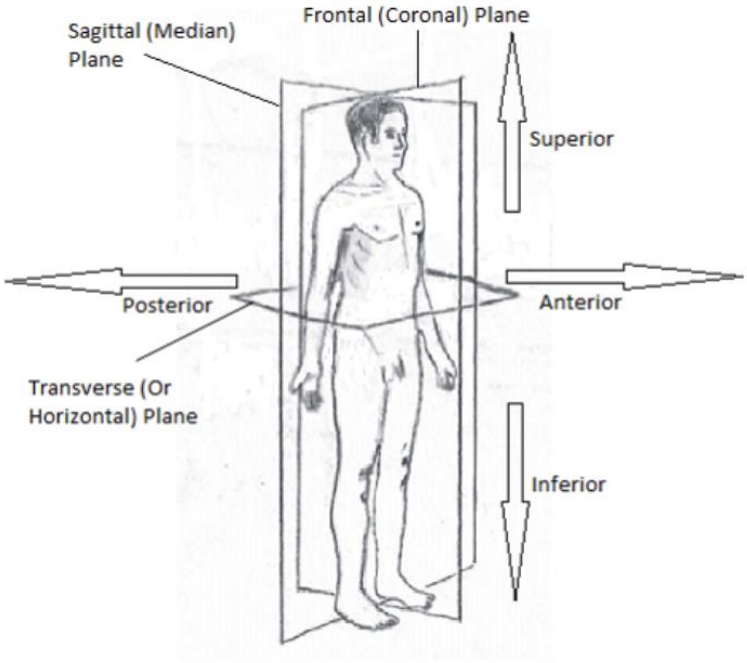

Figure 2: anatomical planes of the body. The motion of each limb of the human body can be described using the following reference planes: sagittal (median), frontal (coronal), transverse (or horizontal) planes.

The joints angles considered for the gait analysis are that of hip, knee, and ankle as we have seen in the previous Section (Figure 1) [26]. Figure 3 shows the different joints movements of the lower limb. Movement in the sagittal plane are flexion/extension and plantar/dorsiflexion for the ankle joint. Movement in the frontal plane is generally defined as abduction/adduction and, for the foot, eversion (that causes the soles to point away from the midline) and inversion (that brings the soles together).

In the transverse plane, finally, there are movements of internal/external rotations [27]. In the present study, there will be particular attention on the movements that describe the kinematics of the hip, knee, and ankle in the frontal plain. The conventions used to specify joint angles [28] are showed in Figure 4.

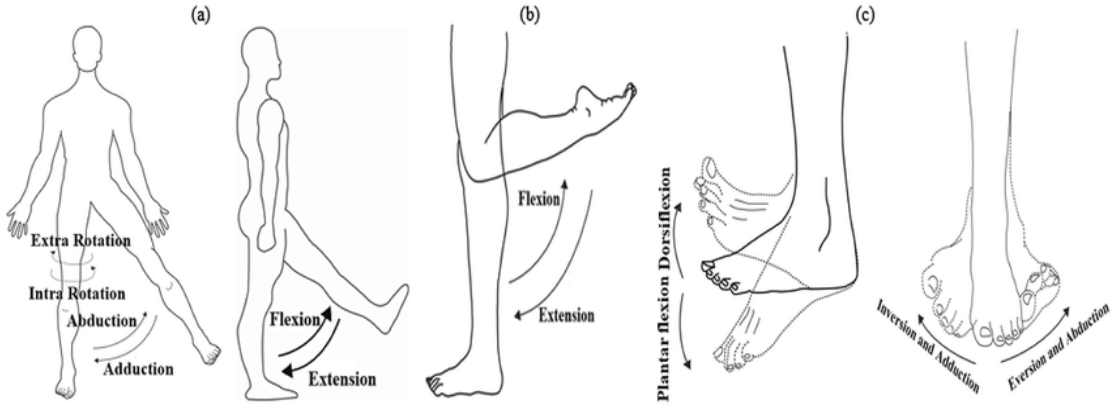

Figure 3: joint movements of the lower limbs. Flexion and extension take place in the sagittal plane (a,b); in the ankle these movements are called dorsiflexion and plantarflexion (c). Abduction and adduction take place in the frontal plane (a) and in the ankle (c) those movements are called inversion (adduction) and eversion (abduction). Internal and external rotation take place in the transverse plane (a). Taken from [27].

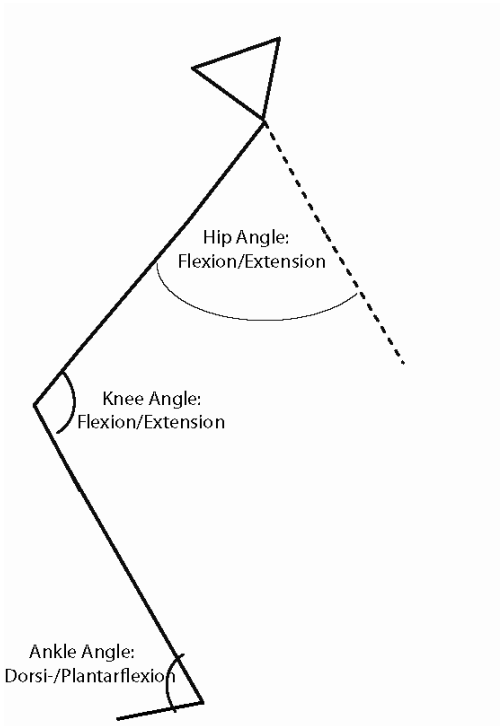

Figure 4: conventions used to specify joints angles. The hip flexion/extension is described by the angle between long axis of pelvis and thigh segment; the knee flexion/extension angle is between long axis of thigh and shank segment; the ankle dorsi/plantarflexion is the angle between the shank and long axis of the foot. Taken from [28].

To estimate hip, knee, and ankle angles, it is necessary the use of protocols. A kinematic protocol is nothing more than a procedure that regulates the acquisition and processing of kinematic data, using a certain marker set and known mathematical conventions. It also ensures that the acquisition method is standardized, and that the measurement is repeatable [29]. Various protocols used for quantitative gait analysis have been implemented to guarantee accuracy and to reduce motion artifacts as the Davis - Helen Hayes protocol [5] (Figure 5), C.A.S.T protocol […], SAFLo protocol [..], the LAMB protocol […]. In the present study, Davis protocol was used because it showed good consistency and small bias for joints flexion/extensions, among the before mentioned protocols [30]. Therefore, it is described in detail below.

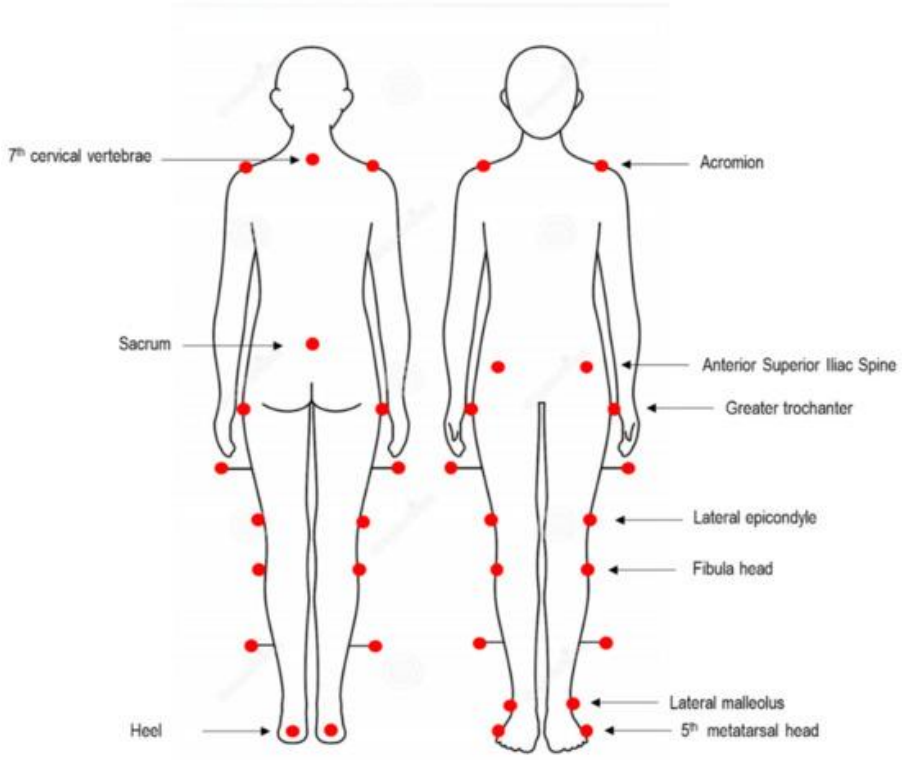

Figure 5: Graphic representation of markers placement according to the protocol proposed by Davis et al. [5], [29]. *Figure adopted from* [29].

After the measurement of some anthropometric measures as [5]:

- body weight
- height
- tibia length
- distance between lateral and medial femoral epicondyles of the knee

- distance between the lateral and medial malleoli of the ankle
- distance between the anterior iliac crests
- pelvis thickness

The protocol requires the placement of reflective markers on some anatomical landmarks and other technical points. Specifically, some markers are directly placed on the skin and in particular:

- three markers placed in the trunk, that are right sternoclavicular junction, left sternoclavicular junction and spinous apophysis;
- three makers are used to describe pelvic motion, such that two markers are placed directly over the left, right anterior superior iliac spine, and one marker is positioned on the sacrum;
- twelve markers are placed on the leg: two markers are placed on the left and right greater trochanter; two markers are placed on the lateral epicondyle of the left, right knee; another two markers are placed at the level of the left and right head of fibula; other two markers are placed on the lateral malleolus along an imaginary line the passes through the transmalleolar axis; moreover, femoral wand and tibial wand are placed on the right and left thigh and shank side to describe their planes with respect to the foot segment;
- four markers are placed on the foot: two markers are located on the second metatarsal head, on the mid-foot side of the equinus break between forefoot and midfoot; the final two markers are located on the calcaneus at the same height above the plantar surface of the foot as the toe markers [5], [31].

Calibration is carried out during the standing phase and consists in acquiring the subject in an upright position for a few seconds. Once the static acquisition has been completed, the dynamic acquisition proceeds, in which the subject walks at normal speed starting from a fixed point [5].

2.3 Main superficial muscles of the lower limb

Proceeding in the proximal-distal direction, there are 4 muscle groups that are part of the lower limb, and they are: hip muscles, thigh muscles, shank muscles and foot muscles [32]. The main muscles of the leg considered for this study are generally involved during gait and their activity can be accurately captured with surface electrodes [33], [34]. In Figure 6 it is shown anterior and posterior muscles of the right leg. We can classify the muscles of the leg according to the number of joints they cross, and to which joints they're acting. Therefore, there are classified as monoarticular and biarticular muscles based on they act on one or two joints [35].

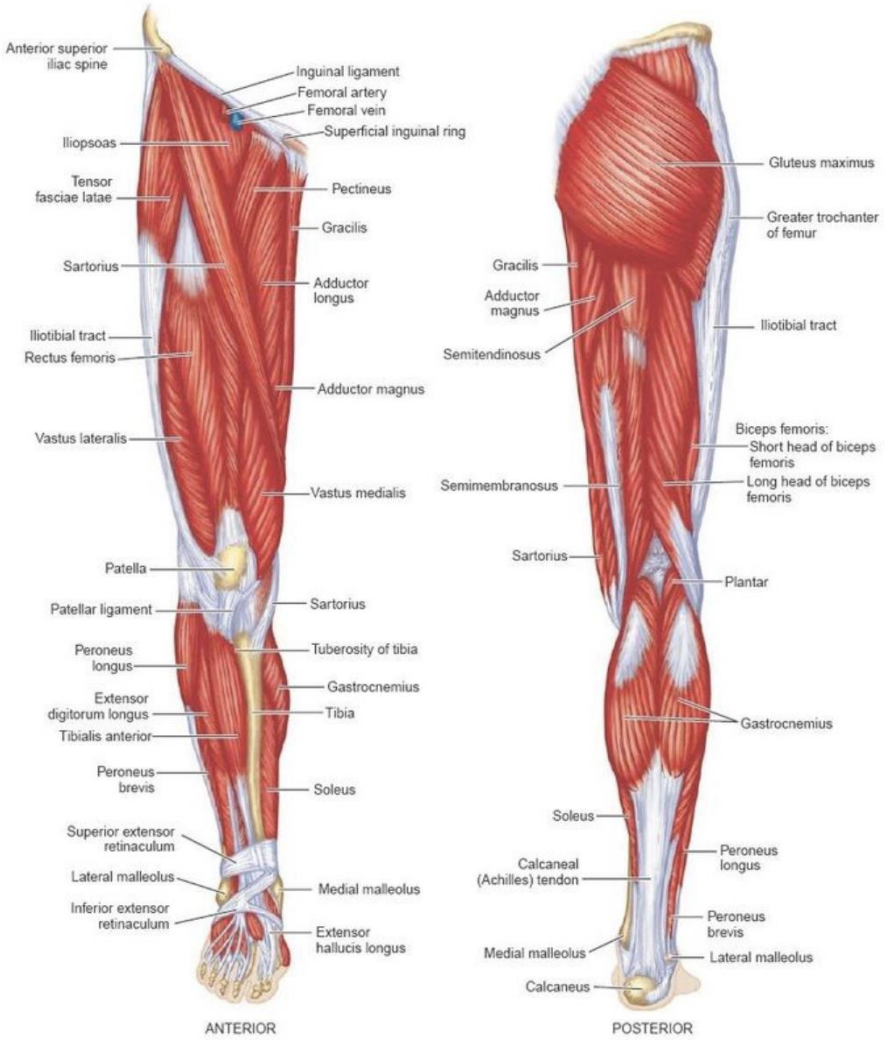

Figure 6: Anterior and posterior muscles of the right leg. Four muscles groups are part of the lower limb, and they are: hip muscles, thigh muscles, shank muscles and foot muscles.

The muscles acting only at the hip joint allow hip movements along the three planes (frontal, sagittal and horizontal) and guarantee stability to the joint itself. Therefore, the hip is able to move the femur and consequently the lower limb, in various directions, following the movements of: flexion/extension, ab/adduction, internal and external rotation of the femur [35].

The muscles of the thigh are constituted, anteriorly, by the quadriceps: rectus femoris, vastus medialis, vastus lateralis and vastus intermedius. The quadriceps, contracting, extend the leg and, with the rectus femoris, participate in the flexion of the thigh as well as, with the knee flexed, in the flexion of the pelvis on the thigh [32].

The muscles acting both at hip and knee joints are: rectus femoris (one of the four muscles of the quadriceps), tensor fasciae latae, sartorius, the hamstrings (semimembranosus, semitendinosus and biceps femoris), gracilis.

The gastrocnemius (medial and lateral), together with the plantaris, are the muscles that act across the knee and ankle joints. The tendon of the gastrocnemius joins with that of the soleus and plantaris to form the Achilles tendon, which inserts into the back of the calcaneus.

The soleus and gastrocnemius together are called the triceps surae acting both at ankle and subtalar joints. The triceps surae, contracting, plantarflexes the foot and rotates it inside; contributes, with the gastrocnemius, to the flexion of the shank on the thigh. Pivoting on the forefoot, the triceps extends the leg over the foot [32].

For what concern the anterior muscles of the shank, we find: tibialis anterior, extensor digitorum longus, peroneus brevis. Tibialis anterior is the most medial of the anterior muscles. It arises from the lateral condyle and the upper half of the lateral fascia of the tibia, bringing its bundles vertically down and crossing the ankle joint. It dorsiflexes, adducts, and medially rotates the foot [32].

A method for analyzing and capturing the electrical activity generated by skeletal muscles' contraction is called electromyography (EMG) [36]. The electrical expression of the neuromuscular activation brought on by a muscle contraction is known as a myoelectric signal. EMG is performed using an instrument called electromyograph to produce a signal called an electromyogram. EMG signals acquired from muscles require advanced methods for onset detection, decomposition, processing, and classification [37]. EMG signals can be used for clinical/biomedical applications, hardware development, and modern human computer interaction. Clinically, EMG is used as diagnostic tool for neurological disorders. In fact, it is frequently being used for assessment of patients with neuromuscular diseases, low back pain and disorders of motor control. Other than physiological and biomechanical research, EMG has been developed as an evaluation tool in applied research, physiotherapy, rehabilitation, sports medicine and training, biofeedback, and ergonomics research [37], [38].

2.4 Hardware and setup

This study was done at the Movement Analysis Laboratory of Università Politecnica delle Marche (UNIVPM), equipped by a motion capture system (BTSEngineering, with sampling rate of 250 Hz) that use 8 digital cameras with powerful infrared illuminators (SMART-DX6000, 2.2 Mpixels, 2048x1088, 340 fps at full resolution) to capture motion in a large measurement volume [5m (l) x 3m (w) x 2m (h)] by guaranteeing accuracy in measurement. Before starting the walking task, each subject is armed of a marker set by a modified Davis protocol and each subject's right leg is provided with EMG electrodes. BTS Bioengineering FREEEMG surface electrodes are employed for this kind of experiment, and they are showed in Figure 7. Using Wi-Fi technology, these probes convert the myoelectric signal produced when muscles contract into an electric digital signal. By doing so, connection wires are minimized, allowing a more comfortable walking task for the subject. Their thin and compact size ensures that they are placed precisely over targeted muscles. To prevent any unwanted movement during a dynamic activity that would contribute random noise to the signal, it is crucial to make sure that each electrode is firmly attached to the skin during the placement phase. To prevent cross-talking occurrences, electrodes must also be placed as close as possible to the muscle's center while maintaining an inter-distance from one another. These electrodes allow the acquisition of EMG data at a sampling rate of 1000 Hz. For each participant, a specific positioning probes protocol was followed. We performed a 6 channels EMG analysis. Figure 8 shows the positioning of EMG electrodes on the right shank. Figure 9 shows the positioning of EMG electrodes on the right thigh and in figure 12 we show the complete EMG electrodes set-up for a representative subject [39]. For what concerns the muscles considered for the analysis, 6 superficial muscles of the right leg are recorded. The first electrode corresponds to TA (Tibialis Anterior); the second electrode is positioned over the GM (Gastrocnemius Medialis) and the third over the GL (Gastrocnemius Lateralis); the fourth electrode is placed on VM (Vastus Medialis) and the fifth over the RF (Rectus Femoris); finally, the sixth and last electrode is positioned on BF (Biceps Femoris caput longus).

The passive and retroreflective markers are located on the subject anatomical landmarks according to Davis protocol showed in Figure 10 and 12: H and B markers are placed over the right and left anterior-superior iliac spine (ASIS), respectively; the sacral H marker is positioned over the subject's posterior-superior iliac spine (PSIS); the right thigh marker set, i.e., the RK, RF, and RH markers, is placed on the subject such that the identified epicondylar axis lies in the plane formed by these three markers (same for the left thigh marker set, i.e. LK, LF and LH); also, the RK and LK markers are positioned along the epicondylar axis and the right and left marker plane are oriented so that the longitudinal axis of the right and left thigh lies in the plane formed by, respectively, the right 3

markers and left 3 markers; the right shank markers, RA, RB and RP are placed on the subject to form another plane in which the epicondylar axis are found (same procedure repeated for the left shank markers, i.e. LA, LB and LP); the RA and LA markers are placed at the level of, but not necessarily over (depending on the subject's tibial rotation characteristics), the lateral malleolus; the toe markers (RT and LT) are placed on the lateral aspect of the foot over the fifth metatarsal head; finally, the heel markers (RQ and LQ) are positioned so that the heel-toe-marker vector is parallel to the sole of the foot and aligned with the foot progression line.

Figure 7: BTS Bioengineering FREEEMG surface electrodes. At left: one of the six surface electrodes used. It is of easy placement and being wires free they let a more comfortable walking task. At right: it is showed the charging box BTS electrodes.

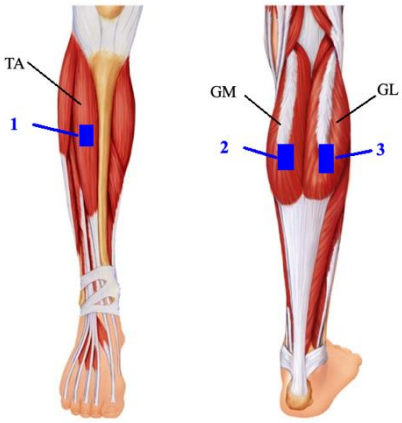

Figure 8: locations of right shank (1,2,3) electrodes with anatomical references of superficial muscles considered for this study. TA: Tibialis Anterior; GM: Gastrocnemius Medialis; GL: Gastrocnemius Lateralis.

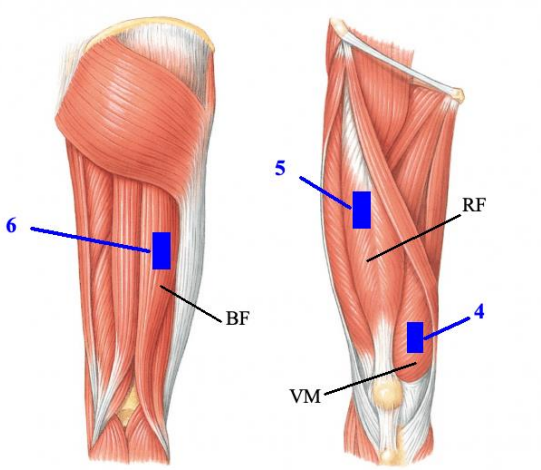

Figure 9: locations of right thigh (4,5,6) electrodes with anatomical references of superficial muscles considered for this study. VM: Vastus Medialis; RF: Rectus Femoris; BF: Biceps Femoris caput longus.

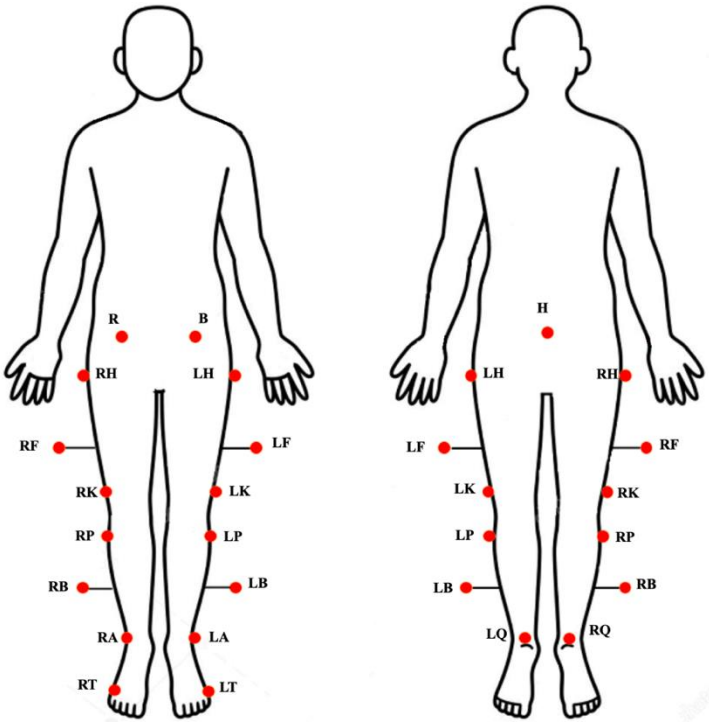

Figure 10: modified Davis protocol used for the study. At the left there is the anterior view of the marker set. At the right it is showed a dorsal view of the subject with the marker set. Taken and modified from [39].

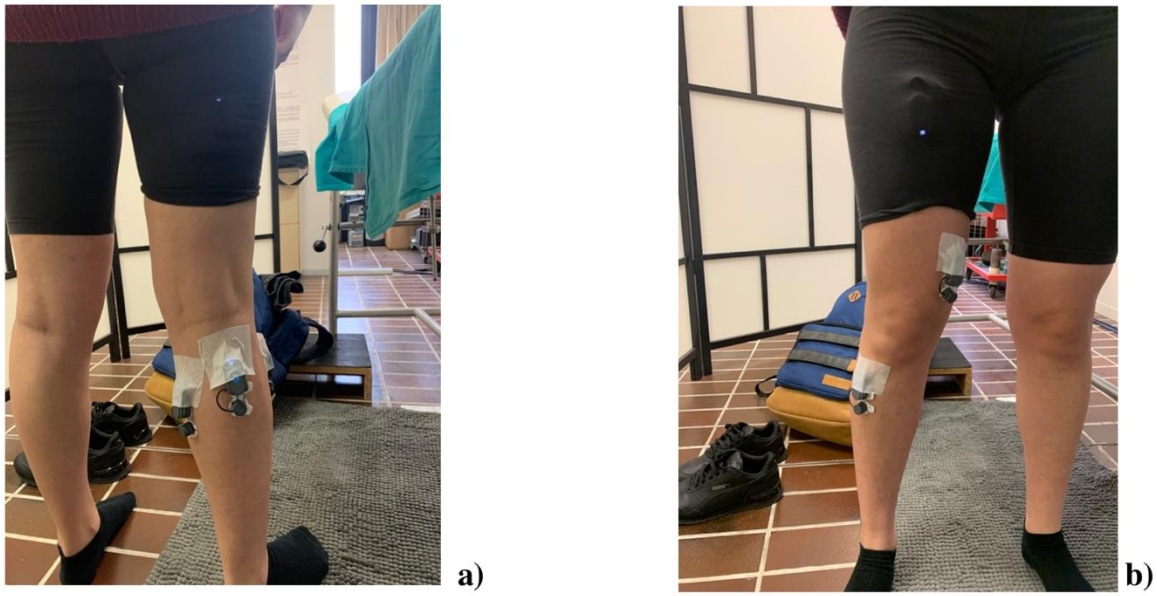

Figure 11: BTS electrodes placement on one subject. In posterior view of the subject (a) there are visible electrodes 2,3 and at the anterior view (b) electrodes 1 and 4 are clearly visible. Electrodes 6 and 5 are covered by subject's shorts.

Figure 12: complete marker set and EMG electrodes set on one subject, anterior (a) and lateral (b) views.

2.5 Definition of walking task

Six healthy adults participated to the study, 4 women and 2 men aged between 25 and 50. All participants are asked to walk on the Laboratory's platform at their comfortable walking speed, doing reversals while performing the test, for a duration of about 2-3 minutes. The time required to perform one task, as the number of steps done are showed in Table 1. Just the right leg was taken in consideration for the analysis, therefore, the number of steps done by each participant and the time required to perform the entire task is referred to this leg. In Figure 13 it is shown the walkway used for the test. No static acquisition was done before the trials, therefore no initial offset angles were removed from the motion angles.

SUBJECTS	*SEX*	*NUMBER OF TRIALS PERFORMED*	*NUMBER OF STEPS*	*TEST TIME*
1	female	1	44	2 min and 15 s
2	female	3	72	3 min
3	female	3	72	3 min
4	male	4	80	4 min and 20 s
5	male	4	80	4 min and 20 s
6	female	3	72	3 min

Table 1: in this table it is shown the number of trials performed by the six subjects, their sex, the average number of steps done on one trial and the average time required to perform one trial. The number of steps is referred to the subjects' right leg.

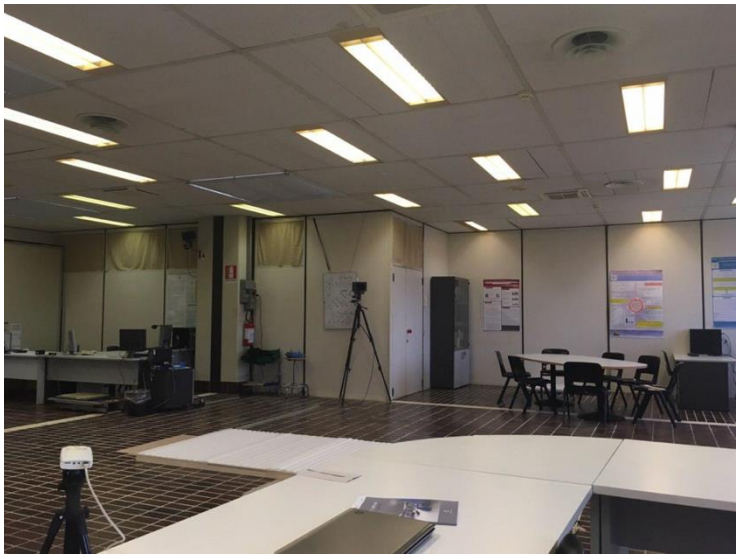

Figure 13: Movement Analysis Laboratory of UNIVPM. Here the six subjects performed the walking task on the platform that is clearly visible in the picture.

2.6 Kinematic data and EMG signal processing

2.6.1 Kinematic data

The analysis of both kinematic data (hip, knee, and ankle angles) and EMG signals were done on the right leg of each participant. Firstly, the kinematic data were filtered with a low-pass Butterworth filter of 2Hz since the power spectrum of all the markers was too low (figure 14, power spectral calculated for heel marker). The extraction of joints angles belonging to the right leg from markers coordinates was done according to the procedure by Davis et al. [5]. The data from ankle, knee and hip angles appeared as depicted in Figure 15. Since the subjects during walking did some reversals, there are present in the signal. Therefore, the next step was simply to exclude from the following analysis the portion of kinematic signal during which each turning is performed. By cutting the signal in the points of initial heel strike and final heel strike for each roundtrip, the entire gait cycles are preserved, and it is possible to obtain a continuous joint motion (Figure 16). The initial and final heel strikes of each roundtrip were found from the vertical component of the heel marker. The last step in

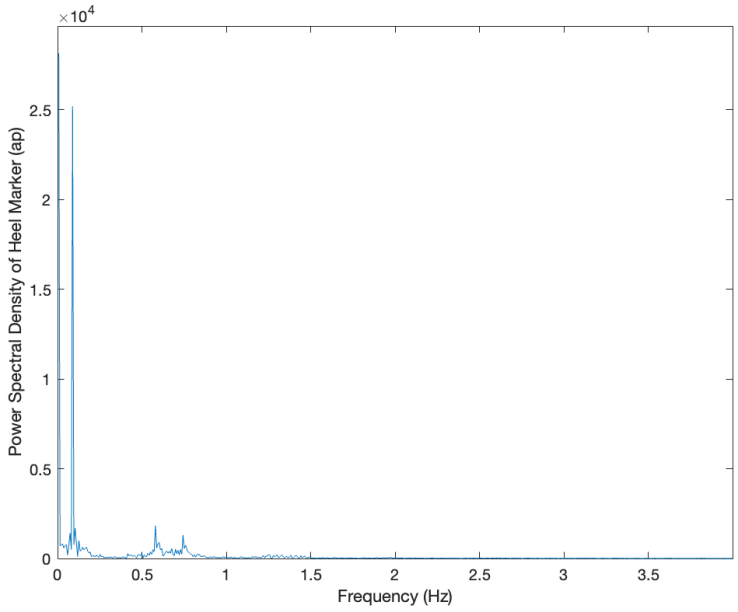

Figure 14: Power Spectral Density of the Anterior-Posterior (ap) component of the heel marker. It is clearly visible the low frequency component of the power spectrum, therefore it was chosen a cut-off frequency of 2 Hz for the Butterworth low-pass filter applied to every marker's raw signal.

kinematic data signal processing, was to resample them from 250 Hz to 25 Hz. In this way, we will have the same number of samples between kinematic data and features vectors of each roundtrip.

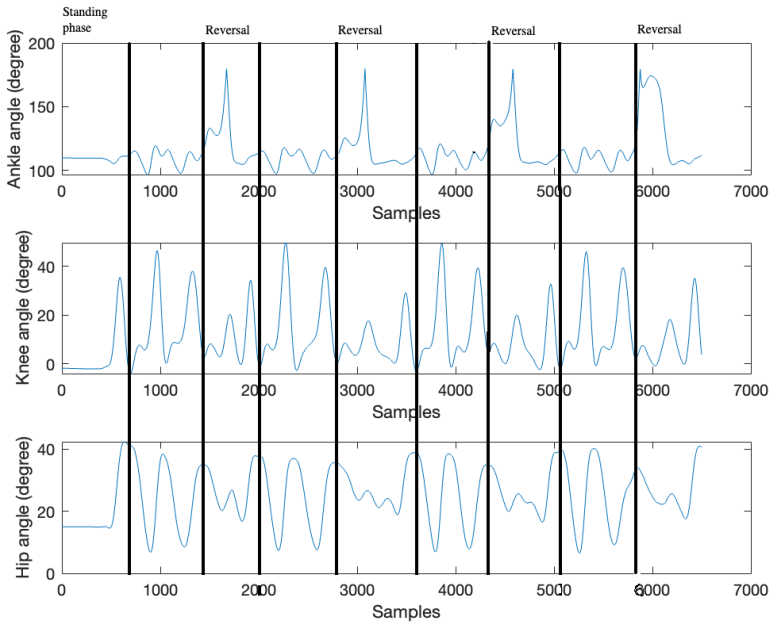

Figure 15: Ankle, knee, and hip angles of the first 6500 samples referred to one subject. Each kinematic signal was cut in the points of initial and final heel strike of each roundtrip, found through the vertical component of the heel marker's coordinates. The standing phase is referred to the time in which the subject was in standing position before starting the walking test, and not referred to the static acquisition, which was not done.

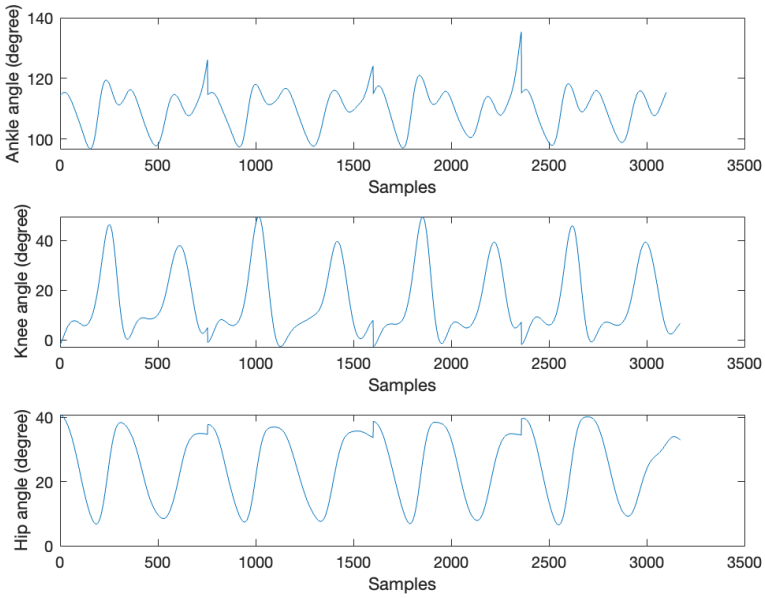

Figure 16: Ankle, knee, and hip joints angles after the cutting phase. Here each roundtrip is joined to obtain a continuous joint motion, without the reversals' phases.

2.6.2 EMG signals and features extraction

The result of the electromyographic acquisition is raw EMG data. Six tracks can be recorded and displayed from a single multi-channel acquisition, as shown in Figure 17. The surface EMG signal acquired at 1000Hz was filtered by a pass band filter with cut off frequencies between 10 and 400 Hz [40].

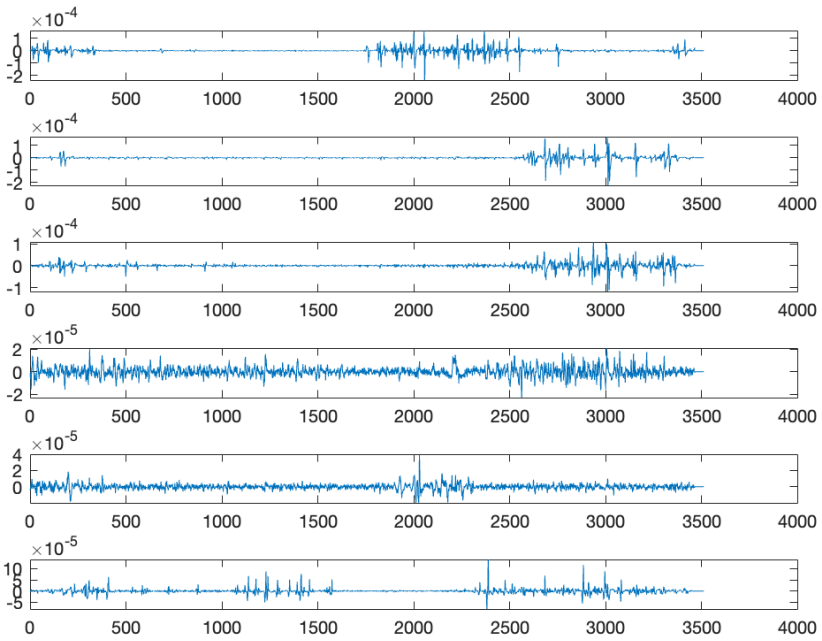

Figure 17: 6 channels recording of a single return. One single acquisition includes 6 channels recording, as shown in figure. Each channel refers to an electrode sensing electrical activity of a different muscle or a group of muscles.

After the filtering phase, it was necessary to cut every EMG channels according to the principle that was applied for kinematic data to delete the reversals phases that were useless for the study. Therefore, the heel strikes of initial and final samples of each roundtrip acquired at a sampling rate of 250 Hz, were transposed into the corresponding samples at EMG sampling rate of 1000 Hz. An example of the way in which EMG data have been cut, is displayed in Figure 18. It is visible the initial and final heel strike samples (that correspond to the event of Initial Contact-IC) of one roundtrip in kinematic signals (here it is reported the knee angle) that corresponds to specifics samples acquired at 1000 Hz.

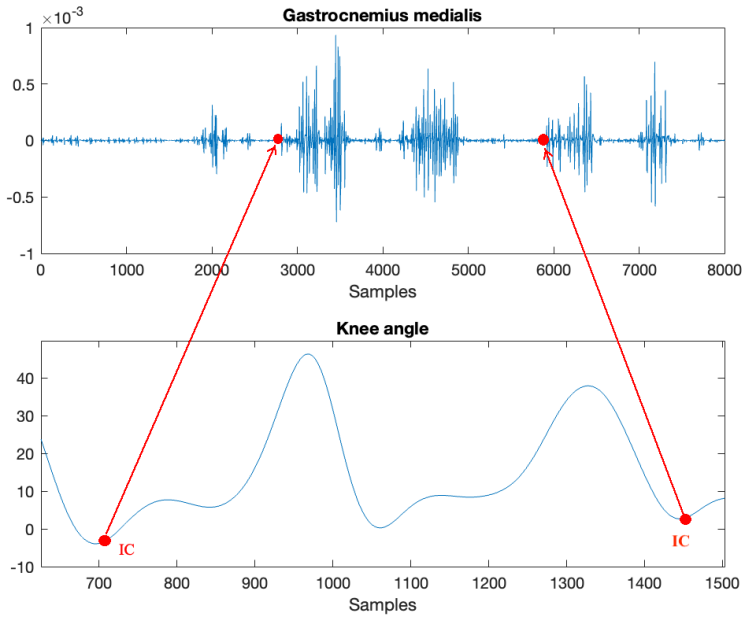

Figure 18: example of EMG signals cutting phase. Here it is reported an example of the way in which EMG channels have been cut, excluding reversals phases that were useless for this study. The kinematic samples (in this example it is displayed the knee angle) corresponding to initial and final heel strikes of each roundtrip (Initial Contact event-IC), were transposed into the corresponding samples at EMG sampling rate of 1000 Hz to conserve the myoelectric information of each roundtrip. The EMG channel displayed in this example is that of Gastrocnemius Medialis (GM, second channel).

EMG signal for each channel have been segmented in each roundtrip before EMG's features calculation. EMG signal is highly variable in nature, and a segmentation approach is required to analyze its random and dynamic pattern. Feeding a myoelectric signal presented as a time sequence, directly to a classifier or a regressor, is impractical, due to the large number of inputs and randomness of the signal. Therefore, the sequence must be mapped into a smaller dimension vector, which is called a feature vector. Features represent raw myoelectric signals useful for regression [41]. A wide spectrum of features has been introduced in literature both for myoelectric classification and regression. Features fall into one of three categories: time domain, frequency (spectral) domain, and timescale (time–frequency) domain [41], [42]. In this study we considered just time domain features, because they have computational simplicity and because they have been widely used in a lot of research and studies [43]. In fact, time domain features are characterized by low computation complexity but contains limited information about the data, while frequency and time-frequency domain features often contain more information about the data, but the disadvantage is that it is often with high computation complexity [14]. In this study, the following time-domain feature set was considered: Mean Absolute Value (MAV), Root Mean Square (RMS), Waveform Length (WL) and Integrated Absolute Value (IAV).

Mean Absolute Value (MAV) is one of the most used features in EMG signal analysis. This feature is an average of absolute value of the EMG signal amplitude in a segment, which can be defined as:

$$MAV = \frac{1}{N}\sum_{i=1}^{N}|x_i| \tag{1}$$

Root Mean Square (RMS) is another frequently used feature. It is modeled as amplitude modulated Gaussian random process whose relates to constant force and non-fatiguing contraction [44]. It is defined as:

$$RMS = \sqrt{\frac{1}{N}\sum_{i=1}^{N}x_i^2} \tag{2}$$

Waveform Length (WL) is defined as cumulative length of the EMG waveform over the time window. It is computed as:

$$WL = \sum_{i=1}^{N-1}|x_{i+1} - x_i| \tag{3}$$

Integrated Absolute Value (IAV) is one of the most effective surface EMG features since it gives a measure of signal amplitude [17]. It is calculated as the summation of the absolute values of the EMG signal amplitude [45], [46]:

$$IAV = \sum_{i=1}^{N}|x_i| \tag{4}$$

Windowing methods are largely adopted to segment and prepare data to further regression analyses in order to calculate EMG's features. Basically, windowing means sub-dividing the entire signal into small parts, with a proper length, from which features will be extracted. Sliding windowing with and without overlapping are two basic types of windowing procedures. In adjacent windowing, windows are taken to a certain length and the following window begins at the end of the previous one. Features are extracted from these windows. However, this windowing method does not provide a dense array of signals, and it's possible that the information is not being fully exploited [47]. In an overlapping window, a predetermined window slides along the entire signal with an increment size fixed that guarantees a percentage of overlapping. By doing so, data from one window is shared with the one next to it [48]. In general, regression or classification accuracy increases as window size increases [49]. In fact, more data will lead to features with lower statistical variance and higher regression/classification precision. The trade-off here should be between a real-time latency and regression/classification accuracy because huge window sizes are substantially more expensive in terms of computational burden (extracting characteristics from large windows requires more power). Typically, window sizes should be examined considering the task being investigated. However, research discover that the upper limit for the window size must be 300ms [50]. Moreover, more recent studies suggest that the window size should optimally be kept between 100-250 ms [51]. In the present work, we set the window size to 200 ms [52], [53], with an overlap of 160 ms (80% of the window dimension). Segmentation is performed over the roundtrips' phases, where myoelectric information is contained.

Once time-domain features (MAV, RMS, WL and IAV) are extracted from sliding windows, they are arranged in a matrix (we obtain one matrix related to each roundtrip) whose number of rows coincides with the total number of segmented windows, and columns contain the value of the features related to all 6 channels. Once the features set is realized, the regressor's input is ready. All the four features are used to train and test regression models. Neural network regressor algorithm is used to predict joints angles, learning from training data (features sets and kinematic data). These signals must be normalized before using neural network. Normalization is an important stage where the range of data will be at the same level or equalize the data range so that no data is more inclined to other attributes [54].Normalization is a technique often applied for preparing data for Machine Learning or Neural Network, in this case. The goal of normalization is to change the values of the numeric columns in the dataset to use a common scale, without distortion in the ranges of values or loss of information. Normalization is also needed for some algorithms to model data correctly. Normalization creates new values that maintain the overall distribution and proportions in the source data, keeping the values within an applied scale in all numeric columns used in the model [55]. In this research we used

standardized score normality or Z-score. Equation 6 is the formula of the Z-score, where χ is the value of each observed data and μ is the average of observed data, and σ is the standard deviation [54].

$$Z - Score(z) = \frac{(\chi - \mu)}{\sigma} \tag{5}$$

As it was said previously, one of the aims of this study is to verify the validity of the Neural Network models for the joints angles regression based on the features obtained from specific and non-specific muscles sets for each joint. This procedure is firstly validated separately for each subject's trials (six regression models were considered for each muscle or group of muscles taken into account), then an inter-trial regression is done (with two regression models for each group of muscles considered). In the next section it is reported a brief description of such architecture.

2.7 Neural Network regression algorithm

A neural network is an artificial neural network (ANN) made up of synthetic neurons or nodes. A neural network can therefore be either a biological neural network consisting of biological neurons, or an artificial neural network intended to address artificial intelligence (AI) issues [56]. Most neural networks have some sort of training rule. In other words, neural networks learn from examples and exhibit some capability for generalization beyond the training data. One deep learning algorithm that mimics the actions of neurons in the human brain is artificial neural networks. Vanilla neural networks, recurrent neural networks, and convolutional neural networks are some examples of artificial neural networks [57]. Only organized data can be handled by vanilla neural networks; in contrast, recurrent neural networks and convolutional neural networks excel at handling unstructured data [57]. Artificial neural networks model biological neuron connections as weights between nodes (Figure 19) [58]. Neural computing requires several neurons, to be connected into a neural network. Each neuron within the network is usually a simple processing unit which takes one or more inputs and produces an output. At each neuron, every input has an associated weight which modifies the strength of each input. The neuron simply adds together all the inputs and calculates an output to be passed on. Neurons are arranged in layers. There are three layers in artificial neural networks: Input layer, Hidden layer, and Output layer. The hidden layer can be more than one in number. A layer has a number of neurons in it. Each layer's neuron will have an associated activation function, that is the function that introduces non-linearity into the relationship. Linear functions are limited because the output is simply proportional to the input. Each layer can also have regularizes associated with it. Regularizes are responsible for preventing overfitting. Artificial neural networks consist of two phases: forward propagation and backward propagation. Forward propagation is the process of multiplying weights with each feature and adding them. The bias is also added to the result. Backward propagation is the process of updating the weights in the model. Backward propagation requires an optimization function and a loss function. An excitatory link is represented by a positive weight, whereas an inhibitory connection is represented by a negative weight. To each input is given a weight before being added together. A linear combination is used to describe this activity. Finally, an activation function regulates the output's amplitude. For instance, a typical acceptable output range is between 0 and 1, however it may be -1 and 1. Neural networks can be used in different fields. The tasks to which artificial neural networks are applied tend to fall within the following broad categories [59]:

- Function approximation, or regression analysis, including time series prediction and modelling.

- Classification, including pattern and sequence recognition, novelty detection and sequential decision making.
- Data processing, including filtering, clustering, blind signal separation and compression.

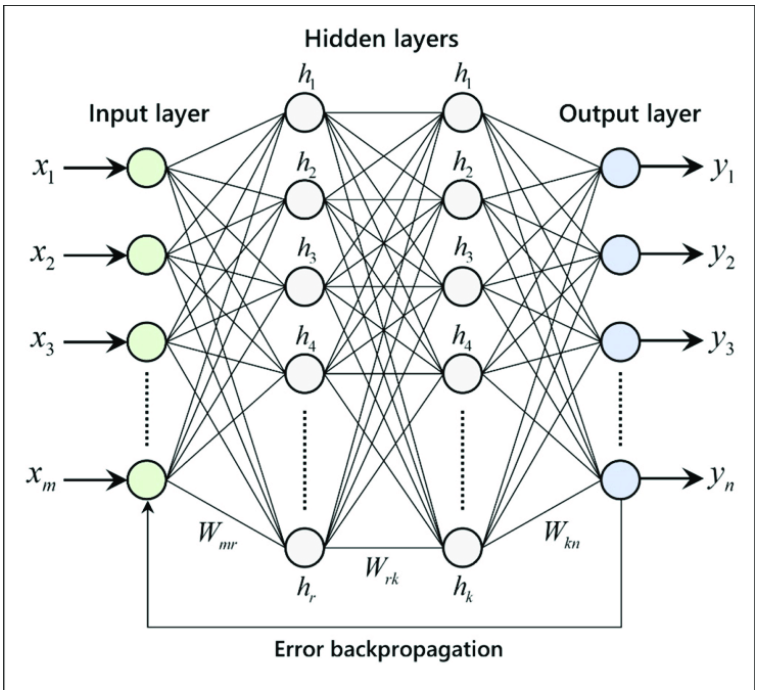

Figure 19: Artificial Neural Network (ANN) structure. It consists of the Input layer, Hidden layers, and Output layer. The learning rule modifies the weights according to the input patterns that is presented with. In a sense, ANNs learn by example as do their biological counterparts. Taken from [58].

In this study we employed a kind of feed-forward Neural Network for regression. A feed-forward neural network is a type of artificial neural network that differs from recurrent neural networks in that connections between nodes do not form loops [60]. This type of neural network was the first and simplest of those developed. Information in this neural network only travels in one direction, forward, with respect to entering nodes, hidden nodes (if any), and exit nodes [61], [62]. Feed-forward networks have no memory of inputs that occurred in previous times, so the output is determined only by the current input. There exist two kinds of feed-forward neural network: single-layer perceptron and multi-layer perceptron. The first kind is the simplest, in fact it consists of a single layer of output nodes, so that the inputs are fed directly to the outputs via a series of weights; each node calculates the sum of the products of the weights and the inputs, and if the value exceeds a predetermined threshold (usually 0), the neuron fires and takes the active value (generally 1), otherwise it takes the

deactivated value (typically -1) [63]. The second type, the multi-layer perceptron, the one taken into account for our study, consists instead of multiple layers of computational units, usually interconnected in a feed-forward way; each neuron in one layer has directed connections to the neurons of the subsequent layer [64].

The structure of the present Neural Network is the one depicted in Figure 20. The first layer (input layer) corresponds to the predictor data (a matrix that contains vectors of all the features plus the response values in a vector Y, that is the joint angle we want to predict). The second layer is the fully connected layer that contains 10 outputs by default. To initialize the weights, it is employed the Glorot initializer (also known as the Xavier initializer) [65]. For each layer, the Glorot initializer independently samples from a uniform distribution with zero mean and variable 2/(I+0), where I is the input size and 0 is the output size of the layer. The third layer is the Rectified Linear Unit (ReLU) activation function that is applied to the first fully connected layer. It performs a threshold operation on each element of the input, where any value less than zero is set to zero, that is:

$$f(x) = \begin{cases} x, & x \geq 0 \\ 0, & x < 0 \end{cases} \tag{6}$$

The fourth layer is the final fully connected layer that has one output; finally, the last layer corresponds to the output, that is the predicted response values.

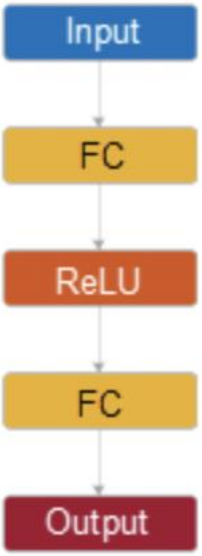

Figure 20: Feed-forward Neural Network. The first fully connected neural network has a connection from the network input (predictor data), and each subsequent layer has a connection from the previous layer. Each fully connected layer multiplies the input by a weight matrix and then adds a bias vector. An activation function follows each fully connected layer, excluding the last. The final fully connected layer produces the network's output, namely predicted response values.

As we have previously explained, the aim of this study is to verify the accuracy of Neural Network regression model considering different amount of data to train and test; secondly, we want to investigate which of the main superficial leg muscles can provide a robust estimation of joints angles respect to others if one considers joint-related muscles and non-joint-related muscles for the regression, once the accuracy of the procedure is verified considering all the muscles configuration (in our study we considered 6 muscles in the complete configuration, see Section 2.4). Two analyses have been performed: regression analysis has been performed firstly on each trial done by the subjects (each trial contains an amount of 44-80 steps, see Table 1) and considering all the six muscles together as well, to evaluate the goodness of the models; secondly, an inter-trial regression analysis was done on each subject. In both the analyses, and for each joint angle's regression, different muscles configurations were taken into account (Table 2).

JOINTS	*JOINT-RELATED MUSCLES*	NON-JOINT-RELATED MUSCLES
ANKLE	-All muscles -Shank muscles -Tibialis anterior -Gastrocnemius medialis and lateralis	-Thigh muscles
KNEE	-All muscles -All muscles without tibialis anterior -Gastrocnemius medialis and lateralis -Vastus medialis -Rectus femoris -Biceps femoris caput longus -Thigh muscles	/
HIP	-All muscles -Rectus femoris and biceps femoris caput longus -Rectus femoris -Biceps femoris caput longus	/

Table 2: muscles configurations for each joint angle's regression.

The models considered for the regression of ankle, knee, and hip on each trial have been six, one for each muscles' configuration and the number of training data and testing data differs between them. Model 1 has 90% training data and 10% testing data; Model 2 has 80% training data and 20% testing data; Model 3 has 70% training data and 30% testing data; Model 4 has 60% training data and 40% testing data; Model 5 has 50% training data and 50% testing data; finally, Model 6 has 40% training data and 60% testing data. For what concern the inter-trial regression, we have two models for each muscles' configuration: Model 1 has 67% of training data (that corresponds to two trials of about 150 steps) and 33% of testing data (that corresponds to one trial of about 70 steps); Model 2 has 33% of training data (one trial) and 67% of testing data (two trials). Only two subjects performed 4 trials each, and for this reason Model 1 and Model 2 were carried out with 3 trials data and 1 left apart in a k-fold manner; thus, the models were tested 4 times. The inter-trial analysis was not done on subject

1, since has performed just one trial (Table 1). The last method consists in a statistical evaluation using the Wilcoxon rank sum test on regressor metrics to recognize the statistical differences between the considered models for Neural Network regression. The Wilcoxon rank sum test is a non-parametric test for two populations when samples are independent [66], [67]. The significance level assumed in this study is 0.05, since it is the common threshold for the p-value in literature [72].

2.8 Regressor performance metrics

To evaluate the performance of neural network regressor, we evaluated 2 classical meters: Root Mean Squared Error (RMSE) and Coefficient of determination (R^2, and pronounced "R squared"). These parameters are calculated for the six models considered for each trial, and then for the two models of intra-subject's regression on each muscles' configurations. On one hand, RMSE describes the typical distance between the predicted value obtained by the regression model and the actual value [68]. On the other hand, R^2 tells us how well the predictor variables can explain the variation in the response variable.

- ***Root Mean Squared Error (RMSE):*** it is the difference between values (sample or population values) predicted by a model or estimator and the values observed. The RMSE is the square root of the second sample moment of the differences between anticipated values and actual values or the quadratic mean of these differences. These deviations are called residuals when the calculations are performed over the data sample that was used for estimation and are called errors (or prediction errors) when computed out-of-sample. The RMSE is used to combine the sizes of predictions' errors for different data points into a single indicator of predictive power [68]. RMSE is a measure of accuracy, and since it is scale-dependent, it should only be used to compare forecasting errors of several models for a single dataset and not between datasets. The 0 number (nearly never attained in practice) would represent a perfect fit to the data, and RMSE is always non-negative. A smaller RMSE is often preferable to a greater one. However, because the measure depends on the scale of the numbers used, comparisons across other types of data would be invalid [69], [70]. RMSE can be computed as:

$$RMSE = \sqrt{\frac{\sum_{i=1}^{N}(X_{obs,i} - X_{pred,i})^2}{N}} \tag{7}$$

- ***Coefficient of determination (R^2):*** It is a metric applied to statistical models whose main objective is to either predict future outcomes or test hypotheses using data from other relevant sources. Based on the percentage of overall variation in outcomes that the model is responsible for explaining, it provides a measure of how effectively observed outcomes are replicated by the model [71]. The coefficient of determination normally ranges from 0 to 1 and it can be expressed in percentage. The most general definition of the coefficient of determination is:

$$R^2 = 1 - \frac{SS_{res}}{SS_{tot}} \tag{8}$$

where: SS_{res} is the sum of squares of the residuals, also called the residual sum of squares:

$$SS_{res} = \sum_i (X_{obs,i} - X_{pred,i})^2 \tag{9}$$

and SS_{tot} is the total sum of squares (proportional to the variance of the data):

$$SS_{tot} = \sum_i (X_{obs,i} - \bar{X})^2 \tag{10}$$

with $\bar{X}$ is the mean of observed data:

$$\bar{X} = \frac{1}{N}\sum_{i=1}^{N} X_{obs,i} \tag{11}$$

3 RESULTS

We can divide this macro-section into two subsections. First subsection describes the results obtained when the regression on each trial is done by varying the number of muscles used for the model. Moreover, additional analysis is done to evaluate the different models based on the different subdivision between training and testing for the data. Then, each of model was tested again to the corresponding testing set. Second subsection shows the results related to inter-trial study, with 2 regressive neural networks models for each muscles' configuration.

3.1 Reduced electrodes setup's impact on overall performance

This section aims to explore the validity of the Neural Network (NN) models for the joints angles regression based on features obtained from specific muscles sets and joint-function related, non-specific muscles sets or non-joint-function related. Table 3 reports regression's results with RMSE (in degrees) and R^2 for the ankle joint, considering the following muscles or groups of muscles: All Muscles (AM), Shank Muscles (SM, i.e., Tibialis Anterior and Gastrocnemius Medialis and Lateralis), Tibialis Anterior (TA), Gastrocnemius Medialis and Lateralis (GML) and Thigh Muscles (TM, i.e., Vastus Medialis, Rectus Femoris and Biceps Femoris). Table 4 shows instead RMSE and R^2 values for the knee joint, considering the following muscles or groups of muscles: All Muscles (AM), All Muscles without Tibialis Anterior (AM without TA), Gastrocnemius Medialis and Lateralis (GML), Vastus Medialis (VM), Rectus Femoris (RF), Biceps Femoris (BF). Table 5 reports RMSE and R^2 values for the hip joint, considering the following muscles or group of muscles: All Muscles (AM), Rectus Femoris and Biceps Femoris (RF and BF), Rectus Femoris (RF), Biceps Femoris (BF). Histograms in Figures 21- 26 allow a visual inspection of these concepts. Additionally, part of the predicted angle using the Model 1 and Model 6 (for AM and TM configurations) and the true angle for ankle, knee and hip (for the hip it is displayed just the predicted angle obtained from Model 1 and Model 6 for AM configuration) are displayed from Figure 27 to 32. It shows that the joints angles during walking can be estimated with great precision using EMG signals, considering all the six muscles. In Tables 3, 4 and 5 results of p-values from the Wilcoxon rank sum test are highlighted comparing R^2 metric between Model 1 and Model 6. Only the models for hip regression considering all muscles in the electrodes' setup revealed to be statistically different in R^2 metric with a p-value lower than 0.05 (p-value of 0.004).

ANKLE	***AM***		***SM***		***TA***		***GML***		***TM***	
	RMSE	R^2	*RMSE*	R^2	*RMSE*	R^2	*RMSE*	R^2	*RMSE*	R^2
MDL 1	2.55±0.49	0.87±0.04	3.02±0.69	0.80±0.09	4.83±0.83	0.53±0.14	3.36±0.75	0.77±0.08	4.77±1.27	0.54±0.19
MDL 2	2.62±0.47	0.86±0.04	3.11±0.64	0.80±0.08	4.86±0.91	0.52±0.15	3.52±0.71	0.75±0.08	4.80±1.33	0.53±0.21
MDL 3	2.56±0.43	0.87±0.03	3.14±0.60	0.79±0.09	4.93±0.92	0.51±0.15	3.44±0.57	0.77±0.06	4.67±1.14	0.56±0.16
MDL 4	2.70±0.49	0.86±0.04	3.25±0.60	0.78±0.09	4.93±0.94	0.51±0.16	3.52±0.60	0.76±0.06	4.82±1.26	0.54±0.18
MDL 5	2.71±0.49	0.85±0.04	3.20±0.66	0.78±0.09	4.90±0.94	0.51±0.16	3.59±0.67	0.74±0.07	4.88±1.28	0.52±0.19
MDL 6	2.83±0.47	0.84±0.04	3.39±0.65	0.76±0.09	4.92±0.94	0.51±0.15	3.66±0.70	0.73±0.08	5.10±1.24	0.48±0.18

Table 3: Mean and standard deviation values of RMSE and R^2 for all the following groups of muscles considered referred to the ankle joint. Here SM, TA and GML are the specific muscles of the ankle joint, while TM are non-specific muscles, considered to study the goodness of the models in the simulated case of trans-amputees' subjects. Statistical evaluation on R^2 metric using the Wilcoxon rank sum test was done between Model 1 and Model 6 (none of the considered models revealed to be statistically different).

KNEE	***AM***		***AM WITHOUT TA***		***GML***		***VM***		***RF***		***BF***		***TM***	
	RMSE	R^2	*RMSE*	R^2	*RMSE*	R^2	*RMSE*	R^2	*RMSE*	R^2	*RMSE*	R^2	*RMSE*	R^2
MDL 1	4.57± 1.29	0.89± 0.06	4.78± 1.00	0.88± 0.06	6.43± 2.30	0.77± 0.15	11.83± 2.63	0.29± 0.19	12.03± 2.79	0.29± 0.11	11.11± 2.72	0.38± 0.16	8.63± 2.47	0.63± 0.11
MDL 2	4.36± 1.03	0.90± 0.04	4.86± 1.25	0.88± 0.04	6.39± 2.23	0.78± 0.14	11.83± 2.44	0.29± 0.19	11.84± 2.86	0.31± 0.13	11.02± 2.74	0.39± 0.18	8.93± 2.65	0.60± 0.14
MDL 3	4.54± 1.08	0.89± 0.03	4.77± 1.13	0.88± 0.03	6.56± 2.31	0.77± 0.13	11.76± 2.45	0.30± 0.19	11.95± 2.59	0.28± 0.18	11.02± 2.61	0.39± 0.16	8.67± 2.20	0.62± 0.11
MDL 4	4.43± 0.90	0.90± 0.03	4.86± 1.07	0.88± 0.03	6.52± 2.41	0.77± 0.14	11.81± 2.38	0.29± 0.19	11.75± 2.88	0.32± 0.13	11.10± 2.53	0.38± 0.16	8.95± 2.50	0.60± 0.14
MDL 5	4.65± 0.99	0.89± 0.03	4.98± 1.17	0.87± 0.04	6.33± 2.49	0.79± 0.14	11.84± 2.42	0.29± 0.19	11.87± 2.91	0.31± 0.13	11.10± 2.66	0.39± 0.17	9.35± 2.60	0.56± 0.15
MDL 6	5.02± 1.31	0.87± 0.04	5.27± 1.28	0.86± 0.04	6.65± 2.35	0.77± 0.13	11.96± 2.41	0.27± 0.21	11.95± 2.88	0.30± 0.14	11.08± 2.56	0.38± 0.17	9.41± 2.96	0.56± 0.18

Table 4: Mean and standard deviation values of RMSE and R^2 for all the following groups of muscles referred to knee joint. Here there are not considered non-specific muscles for the knee joint, but it has been taken TM for the regression analysis to evaluate the goodness of the models to simulate the case of trans-amputees' subjects. Statistical evaluation on R^2 metric using the Wilcoxon rank sum test was done between Model 1 and Model 6 (none of the considered models revealed to be statistically different).

HIP	***AM***		***RF AND BF***		***RF***		***BF***	
	RMSE	R^2	*RMSE*	R^2	*RMSE*	R^2	*RMSE*	R^2
MDL 1	3.25±0.88	0.91±0.03**	5.57±1.67	0.74±0.10	7.25±1.90	0.55±0.16	8.40±2.61	0.41±0.22
MDL 2	3.35±0.87	0.90±0.04	5.74±1.66	0.72±0.11	7.13±1.96	0.57±0.16	8.43±2.65	0.40±0.23
MDL 3	3.38±0.80	0.90±0.04	5.71±1.57	0.72±0.09	7.10±2.00	0.57±0.17	8.43±2.54	0.40±0.21
MDL 4	3.48±0.81	0.90±0.03	5.75±1.56	0.72±0.09	7.19±1.97	0.55±0.17	8.46±2.43	0.40±0.20
MDL 5	3.51±0.84	0.89±0.03	5.79±1.66	0.72±0.10	7.21±2.02	0.55±0.17	8.52±2.50	0.39±0.20
MDL 6	3.80±0.97	0.88±0.04**	5.95±1.67	0.70±0.10	7.25±2.03	0.55±0.17	8.56±2.56	0.38±0.21

*Table 5: Mean and standard deviation values of regression performance metrics RMSE and R^2 for the hip joint considering all the following groups of muscles. Statistical evaluation on R^2 metric using the Wilcoxon rank sum test between Model 1 and Model 6 is added (** models with p-value < 0.05).*

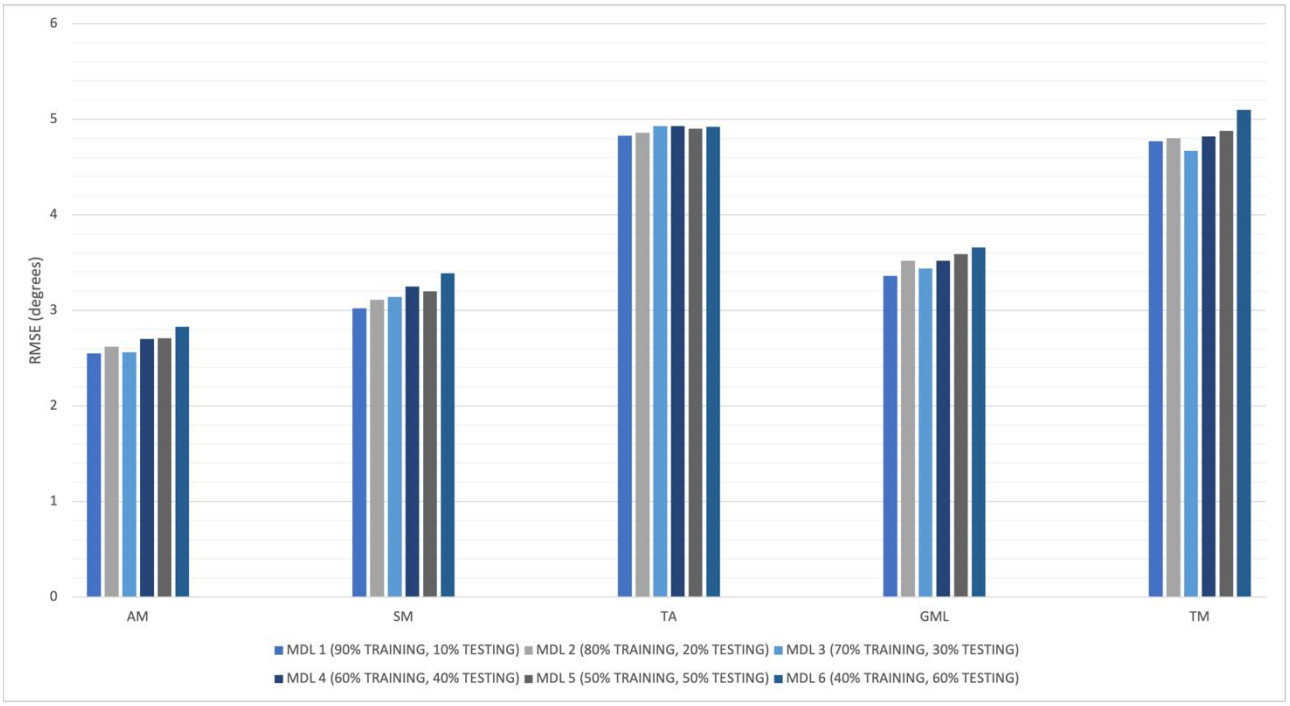

Figure 21: Histogram of RMSE obtained for ankle joint. The RMSE is higher than 4° if one considers just the tibialis anterior muscle in the electrodes' configuration, while if only the muscles of the shank are considered, comparable results can be achieved with respect to the initial configuration with all the six muscles. If distal muscles respect to the ankle joint are chosen (the muscles of the thigh), RMSE remains still lower than 6°.

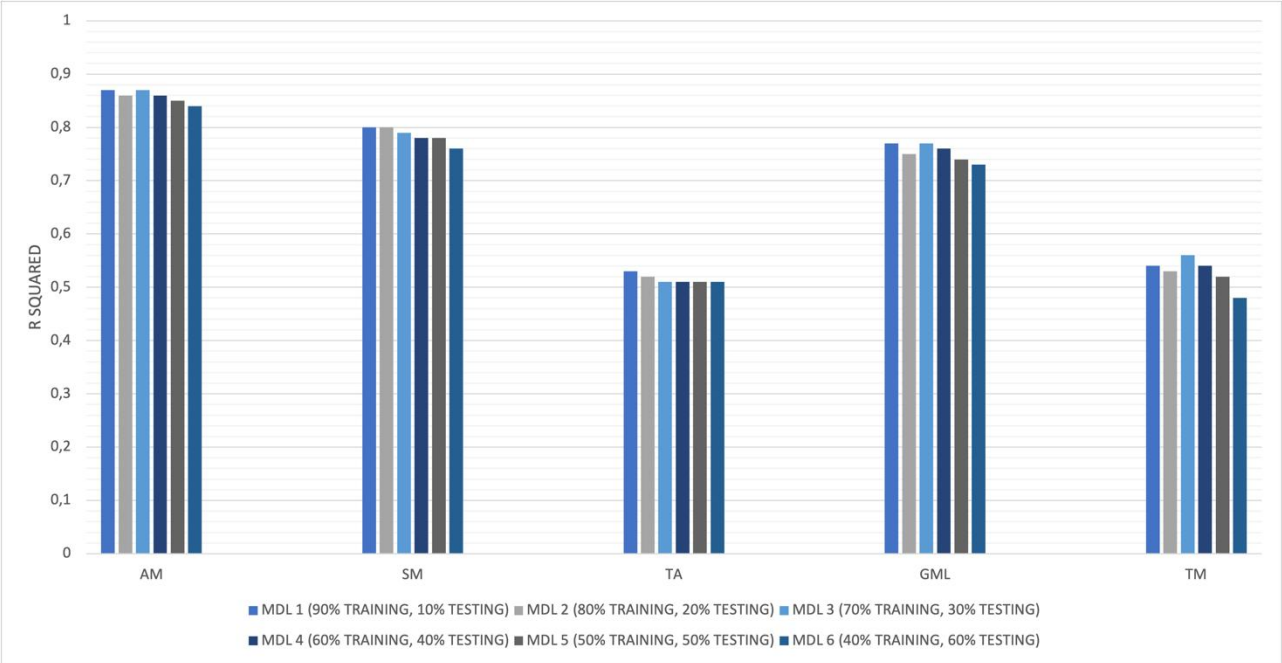

Figure 22: Histogram of R^2 obtained for ankle joint. Here the R-Squared obtained for the ankle angle regression reaches values very close to 0.90 considering all the six muscles; choosing only the muscles of the shank, the R-Squared remains still high and around 0.80; R-Squared is diminished instead considering the muscles of the thigh, with R-Squared lower than 0.60.

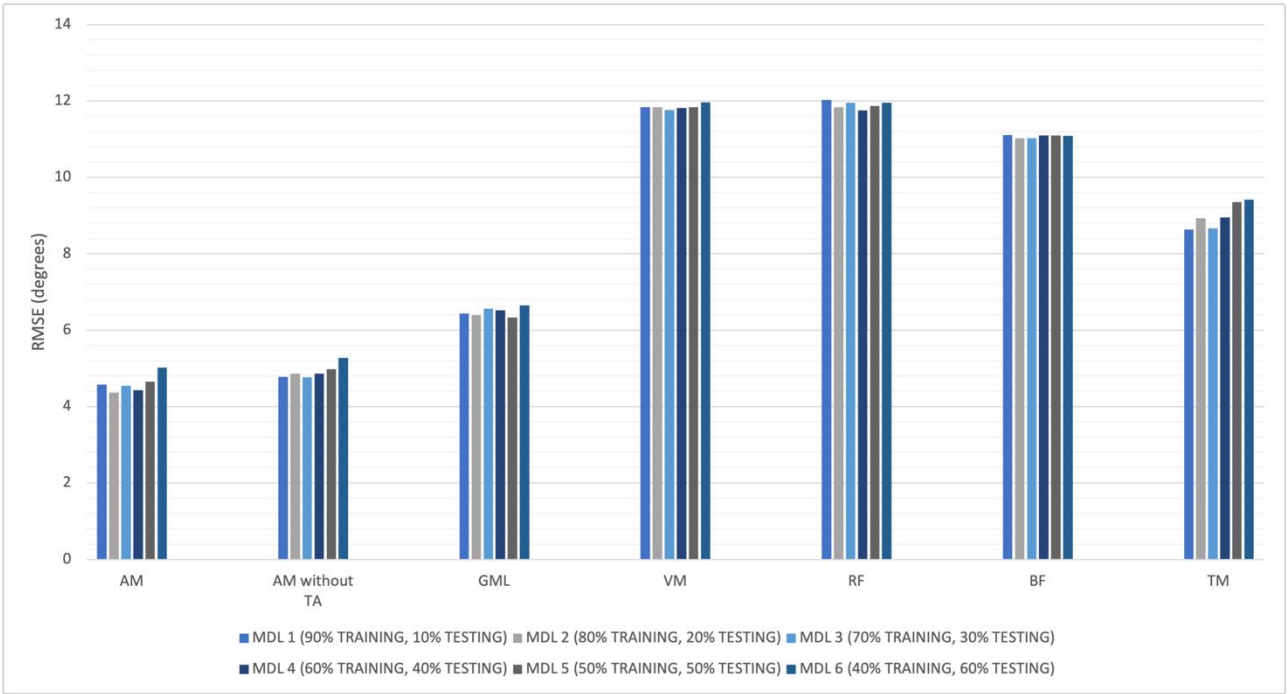

Figure 23: Histogram of RMSE obtained for knee joint. Best results are achieved from the initial configuration with the six muscles (4°<RMSE<6°); excluding the tibialis anterior muscle, the results obtained are comparable to the initial configuration. RMSE remains higher for the other groups of muscles considered, and choosing the muscles of the thigh, regression performance is diminished, with a RMSE higher than 6°.

Figure 24: Histogram of R^2 obtained for knee joint. From the initial configuration with all the six muscles, R-Squared is high, with values for all the six models that remains around 0.90; comparable results are obtained excluding the tibialis anterior muscle. Choosing the muscles of the thigh, the R-Squared reaches values lower than 0.70.

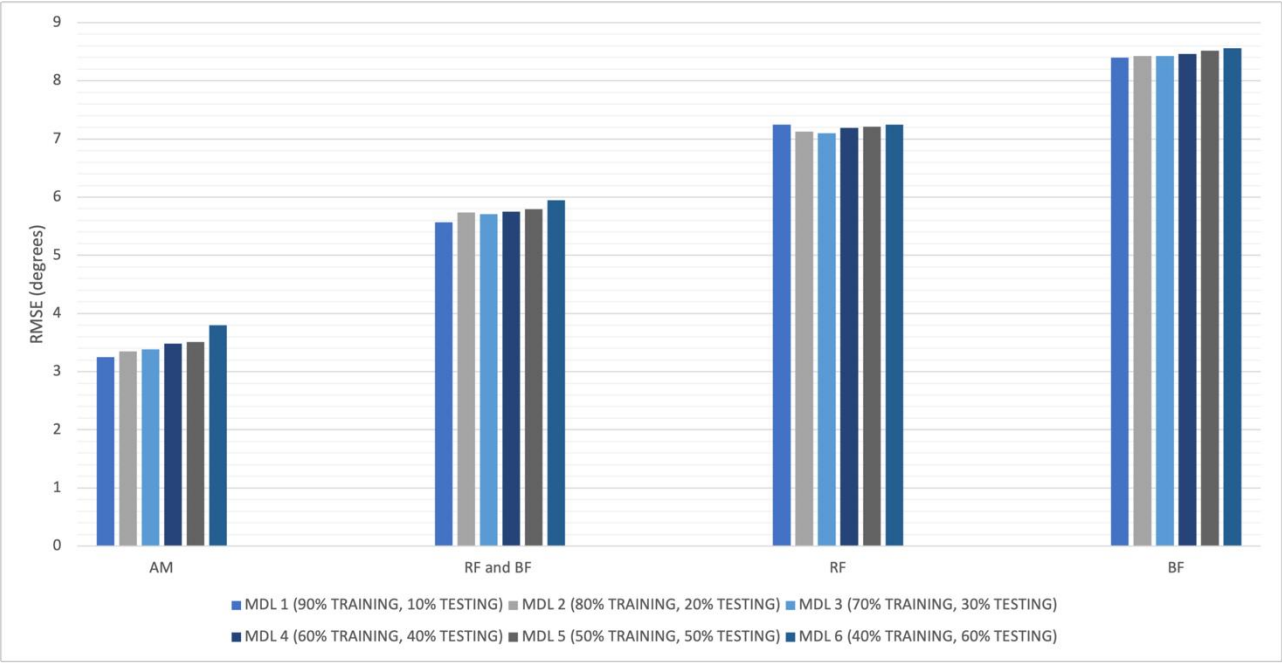

Figure 25: Histogram of RMSE obtained for hip joint. Best results are achieved from all muscles configuration (3°<RMSE<4°). The other muscles configurations chosen to regress hip angle, are those with muscles that cross the hip joint (RF and BF): from those, it was obtained an RMSE higher than 5°.

Figure 26: Histogram of R^2 obtained for hip joint. Best results are achieved if one considers all the six muscles with R-Squared around 0.90. R-Squared obtained from the two muscles that cross the hip joint together reaches values close to 0.70, while if RF and BF are considered alone for the regression, the R-Squared obtained is lower than 0.60.

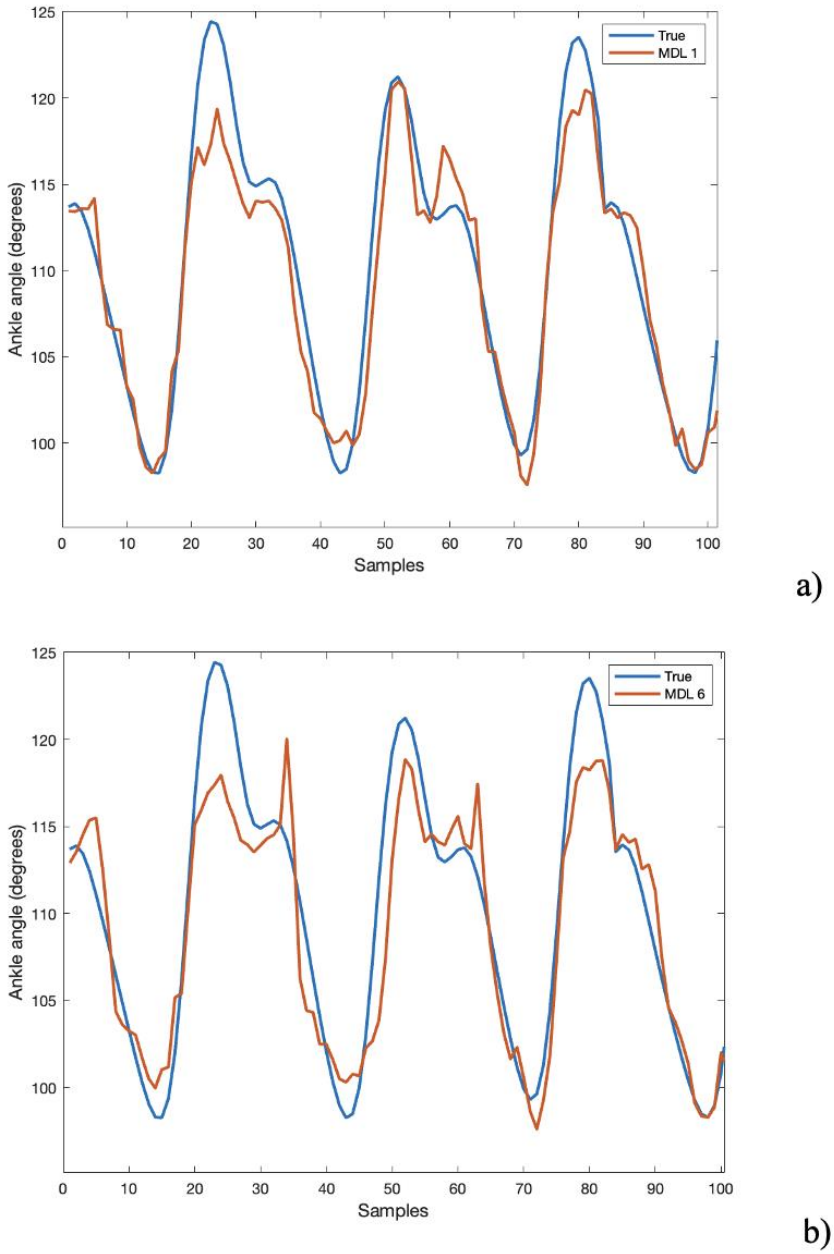

Figure 27: The estimated angle and true angle of the ankle using Neural Networks regression Model 1 (a) and Model 6 (b), considering all the six muscles.

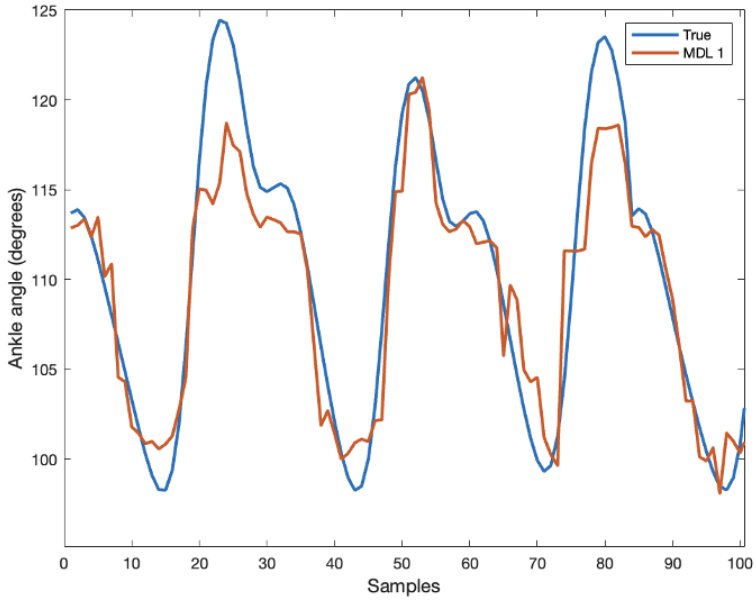

a)

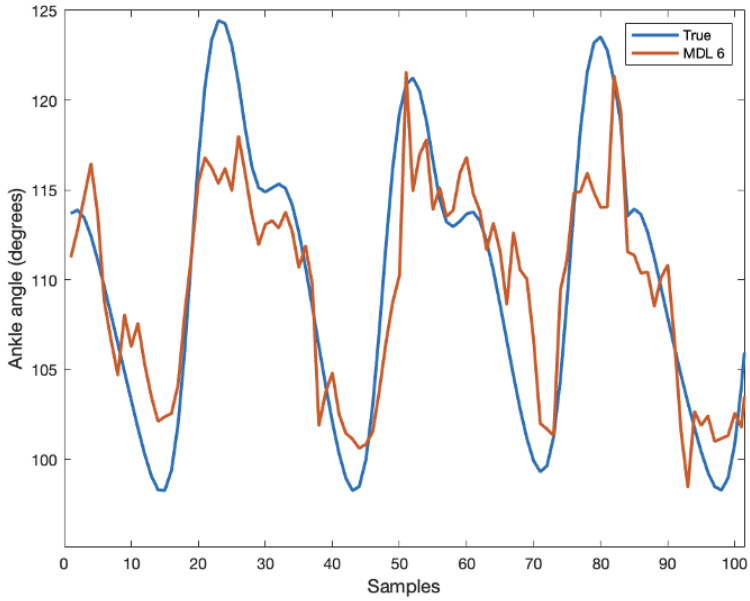

b)

Figure 28: The estimated angle and true angle of the ankle using Neural Networks regression Model 1 (a) and Model 6 (b), considering the muscles of the thigh.

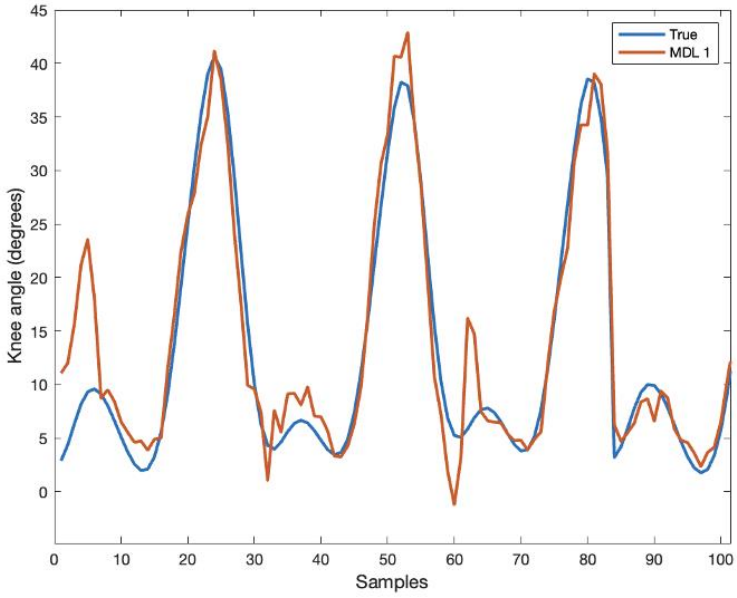

a)

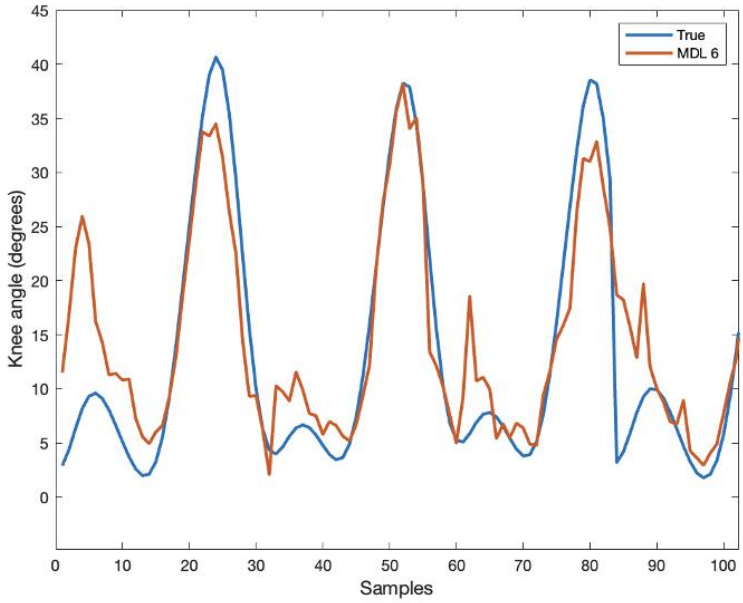

b)

Figure 29: The estimated angle and true angle of the knee using Neural Networks regression Model 1 (a) and Model 6 (b), considering all the six muscles.

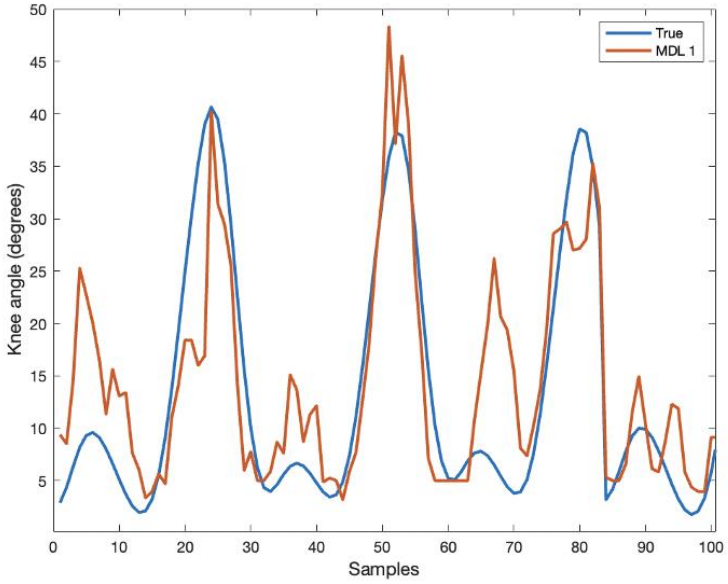

a)

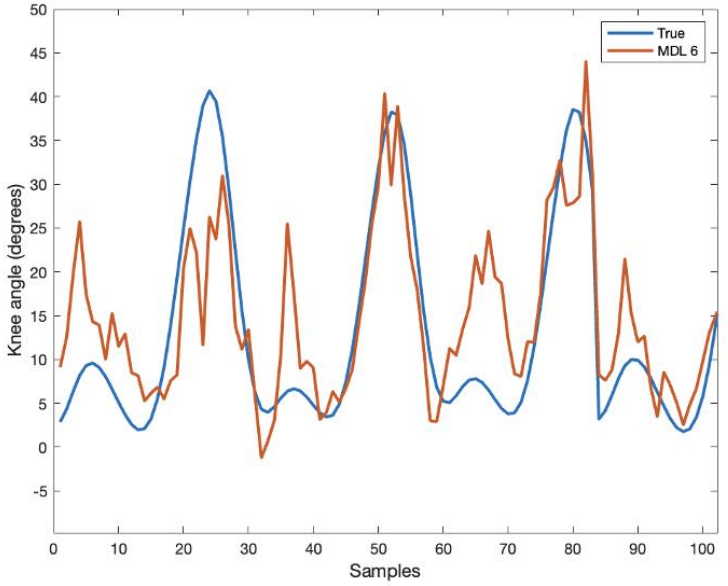

b)

Figure 30: The estimated angle and true angle of the knee using Neural Networks regression Model 1 (a) and Model 6 (b), considering the muscles of the thigh.

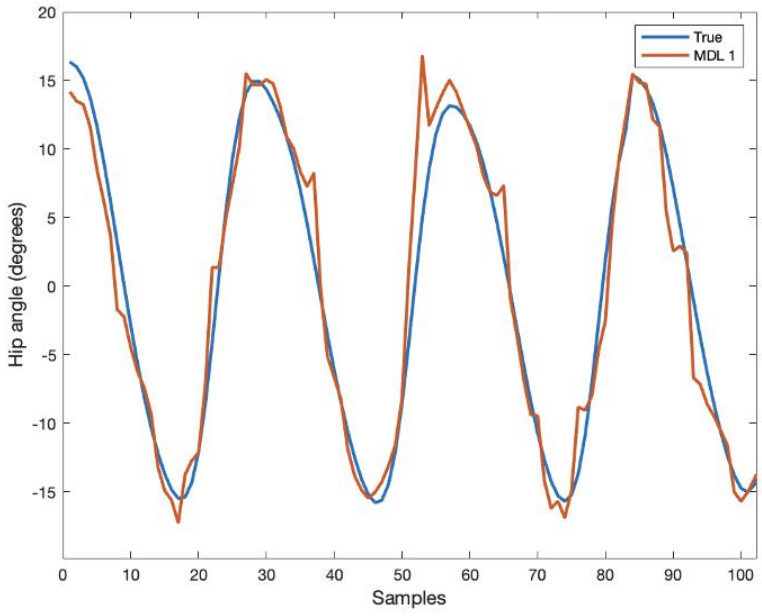

a)

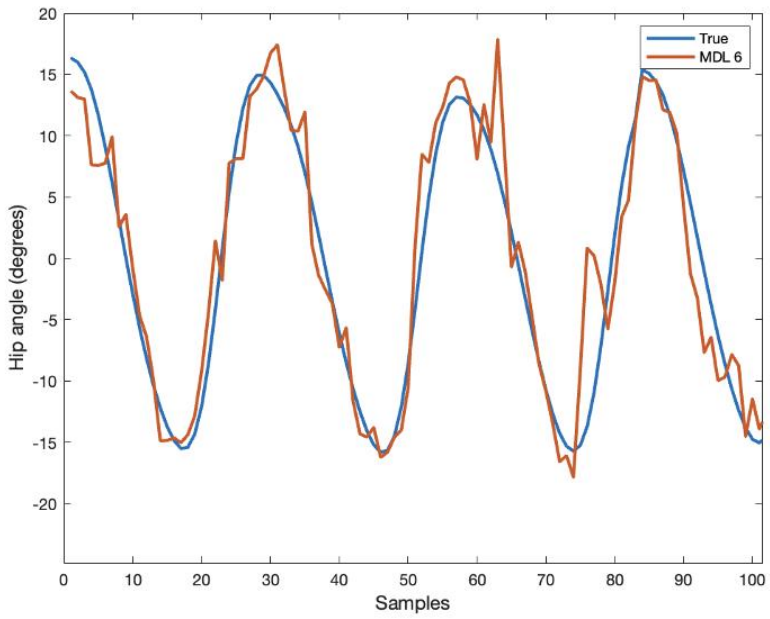

b)

Figure 31: The estimated angle and true angle of the hip using Neural Networks regression Model 1 (a) and Model 6 (b), considering all the six muscles.

In this section, the results obtained re-testing the models with training data sets are appended as well, and they are indicated in Table 6, 7 and 8.

ANKLE	***AM***		***SM***		***TA***		***GML***		***TM***	
	RMSE	R^2	*RMSE*	R^2	*RMSE*	R^2	*RMSE*	R^2	*RMSE*	R^2
MDL 1	1.95±0.37	0.92±0.04	2.73±0.62	0.85±0.10	4.59±0.79	0.57±0.15	3.22±0.72	0.79±0.08	4.11±1.09	0.66±0.23
MDL 2	1.98±0.35	0.92±0.04	2.75±0.57	0.85±0.09	4.53±0.85	0.58±0.17	3.21±0.65	0.79±0.08	4.03±1.12	0.67±0.27
MDL 3	1.90±0.31	0.93±0.03	2.72±0.52	0.85±0.10	4.64±0.88	0.56±0.17	3.16±0.52	0.80±0.06	4.03±0.98	0.67±0.19
MDL 4	1.89±0.34	0.93±0.04	2.67±0.49	0.86±0.10	4.52±0.86	0.58±0.17	3.13±0.53	0.80±0.06	3.93±1.03	0.68±0.23
MDL 5	1.82±0.32	0.93±0.04	2.64±0.55	0.86±0.10	4.49±0.86	0.59±0.19	3.16±0.59	0.80±0.08	3.89±1.02	0.69±0.25
MDL 6	1.70±0.28	0.94±0.03	2.66±0.53	0.86±0.10	4.46±0.85	0.59±0.17	3.14±0.60	0.80±0.09	3.84±0.93	0.70±0.26

Table 6: Mean and standard deviation of RMSE and R^2 results for training data.

KNEE	***AM***		***AM WITHOUT TA***		***GML***		***VM***		***RF***		***BF***		***TM***	
	RMSE	R^2	*RMSE*	R^2	*RMSE*	R^2	*RMSE*	R^2	*RMSE*	R^2	*RMSE*	R^2	*RMSE*	R^2
MDL 1	3.07± 0.87	0.95± 0.03	3.34± 0.70	0.94± 0.04	5.52± 1.97	0.83± 0.16	11.05± 2.46	0.38± 0.25	11.26± 2.58	0.38± 0.14	10.33± 2.53	0.47± 0.20	7.19± 2.06	0.74± 0.13
MDL 2	2.95± 0.70	0.96± 0.02	3.39± 0.80	0.94± 0.03	5.56± 1.94	0.83± 0.14	11.,09± 2.29	0.38± 0.25	11.24± 2.72	0.39± 0.16	10.25± 2.55	0.47± 0.21	7.26± 2.15	0.74± 0.12
MDL 3	2.93± 0.70	0.96± 0.02	3.21± 0.76	0.95± 0.02	5.53± 1.95	0.84± 0.12	11.04± 2.30	0.38± 0.24	11.24± 2.44	0.39± 0.25	10.28± 2.43	0.48± 0.19	7.20± 1.83	0.74± 0.15
MDL 4	2.75± 0.59	0.96± 0.02	3.15± 0.69	0.95± 0.03	5.65± 2.09	0.83± 0.13	10.98± 2.21	0.39± 0.26	11.18± 2.74	0.40± 0.16	10.23± 2.33	0.48± 0.19	7.00± 1.96	0.76± 0.16
MDL 5	2.80± 0.60	0.96± 0.02	3.09± 0.73	0.95± 0.03	5.24± 2.06	0.85± 0.10	10.93± 2.23	0.39± 0.26	11.12± 2.73	0.40± 0.15	10.30± 2.47	0.47± 0.18	6.97± 1.94	0.76± 0.13
MDL 6	2.64± 0.69	0.97± 0.02	2.98± 0.72	0.96± 0.02	5.28± 1.87	0.85± 0.12	10.90± 2.20	0.40± 0.31	11.04± 2.66	0.41± 0.16	10.16± 2.35	0.48± 0.18	6.72± 2.11	0.77± 0.13

Table 7: Mean and standard deviation of RMSE and R^2 results for training data.

HIP	***AM***		***RF AND BF***		***RF***		***BF***	
	RMSE	R^2	*RMSE*	R^2	*RMSE*	R^2	*RMSE*	R^2
MDL 1	2.23±0.60	0.96±0.02	4.84±1.45	0.80±0.12	6.78±1.78	0.61±0.18	7.92±2.46	0.47±0.25
MDL 2	2.16±0.56	0.96±0.01	4.85±1.40	0.80±0.10	6.77±1.86	0.61±0.19	7.78±2.45	0.49±0.28
MDL 3	2.16±0.51	0.96±0.01	4.81±1.32	0.81±0.09	6.76±1.90	0.61±0.18	7.77±2.34	0.49±0.26
MDL 4	2.08±0.48	0.96±0.02	4.74±1.29	0.81±0.08	6.75±1.85	0.61±0.18	7.74±2.22	0.50±0.25
MDL 5	2.01±0.48	0.97±0.01	4.69±1.34	0.81±0.08	6.71±1.88	0.62±0.17	7.80±2.29	0.49±0.25
MDL 6	1.94±0.50	0.97±0.01	4.53±1.27	0.83±0.09	6.59±1.85	0.63±0.15	7.70±2.30	0.50±0.28

Table 8: Mean and standard deviation of RMSE and R^2 results for training data.

3.2 Inter-trial analysis

The last point of this study addressed is how the overall regression performance is influenced in inter-trial analysis, when the same training/testing data are referred to the same subject but to different trials. The aim is to verify the efficacy of the NN models when doing regression on an entire trial or two trials (corresponding, respectively, to about 70 or 150 steps) of the same subject that is used as training data to be tested on one or two trials performed by the same subject. Mean values of the metrics obtained for Model 1 and Model 2 were calculated. Specific evaluations are performed defining models with the above-mentioned subdivision for training and testing but considering a specific set of electrodes. The muscles or group of muscles taken into account were the same considered for the previous analysis for the ankle, knee and hip angles regression.

Table 9, 10 and 11 shows the results obtained for each joint angle with the performance of statistical evaluation on R^2 metric. It is showed statistically differences in R^2 metric between Model 1 and Model 2 for the ankle angle regression considering all muscles in the overall electrodes' setup with a p-value lower than 0.05. Histograms in Figures 32, 33, 34, 35, 36 and 37 allow a visual inspection of these aspects. Additionally, part of the predicted angle using the two models (for ankle and knee both in AM and TM configurations) and the true angle for ankle, knee and hip (for the hip it is displayed just the predicted angle from AM configuration) are displayed in Figures 38, 39, 40, 41 and 42.

ANKLE	***AM***		***SM***		***TA***		***GML***		***TM***	
	RMSE	R^2	*RMSE*	R^2	*RMSE*	R^2	*RMSE*	R^2	*RMSE*	R^2
MDL 1	2.85±0.47	0.84±0.04**	3.32±0.48	0.79±0.05	4.93±0.60	0.53±0.09	3.65±0.61	0.74±0.08	4.89±1.11	0.52±0.19
MDL 2	3.45±1.34	0.75±0.23**	3.96±1.35	0.68±0.24	5.38±0.91	0.44±0.16	4.37±1.48	0.61±0.26	5.36±1.45	0.42±0.30

*Table 9: Mean and standard deviation values of RMSE and R^2 metrics for the ankle joint. As in the previous section, here we consider as well both specific (SM, TA and GML) and non-specific (TM) muscles of the ankle. Statistical evaluation on R^2 metric using the Wilcoxon rank sum test between Model 1 and Model 2 is added (** models with p-value < 0.05).*

KNEE	AM		AM WITHOUT TA		GML		VM		RF		BF		TM	
	RMSE	R^2	RMSE	R^2	RMSE	R^2	RMSE	R^2	RMSE	R^2	RMSE	R^2	RMSE	R^2
MDL 1	4.55± 1.58	0.87± 0.05	4.64± 1.46	0.87± 0.05	6.00± 1.37	0.78± 0.07	11.29± 2.36	0.22± 0.16	10.98± 2.90	0.29± 0.12	10.15± 2.55	0.38± 0.14	7.92± 2.52	0.63± 0.12
MDL 2	5.53± 3.47	0.80± 0.22	5.92± 3.50	0.78± 0.23	6.78± 3.06	0.71± 0.20	11.86± 2.94	0.15± 0.20	11.23± 3.26	0.26± 0.17	10.64± 2.90	0.32± 0.15	8.75± 3.53	0.55± 0.22

Table 10: Mean and standard deviation values of RMSE and R^2 metrics for the knee joint. Statistical evaluation on R^2 metric using the Wilcoxon rank sum test was done between Model 1 and Model 2 (none of the considered models revealed to be statistically different).

HIP	AM		RF AND BF		RF		BF	
	RMSE	R^2	RMSE	R^2	RMSE	R^2	RMSE	R^2
MDL 1	3.38±1.32	0.89±0.06	5.37±1.82	0.72±0.11	6.78±2.30	0.55±0.20	7.21±2.40	0.49±0.19
MDL 2	4.11±2.58	0.82±0.22	5.74±2.03	0.68±0.13	7.07±2.46	0.52±0.20	7.52±2.55	0.46±0.19

Table 11: Mean and standard deviation values of RMSE and R^2 metrics for the hip joint. Statistical evaluation on R^2 metric using the Wilcoxon rank sum test was done between Model 1 and Model 2 (none of the models revealed to be statistically different).

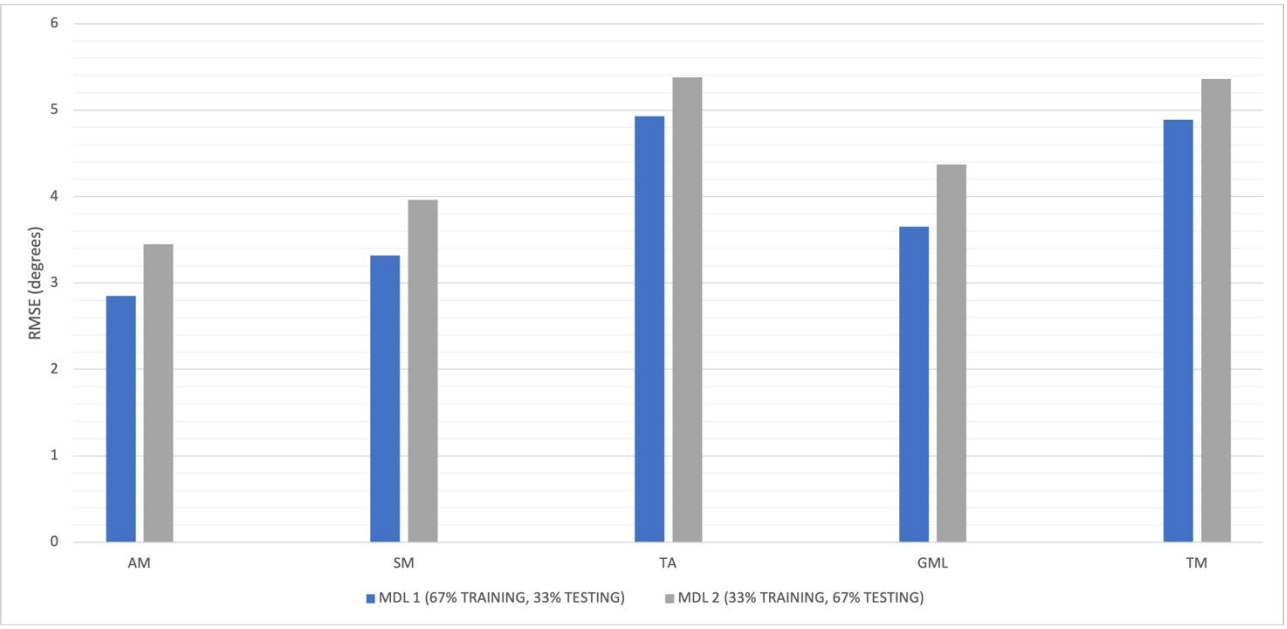

Figure 32: Histogram of RMSE obtained for the ankle joint. From the initial configuration with all the six muscles, it is obtained an RMSE with values close to 3°; comparable results are obtained if only the muscles of the shank are considered for the ankle angle regression, with RMSE that remains lower than 4°. Choosing distal muscles with respect to the ankle joint (the muscles of the thigh), the RMSE obtained has values around 5° for both Model 1 and Model 2.

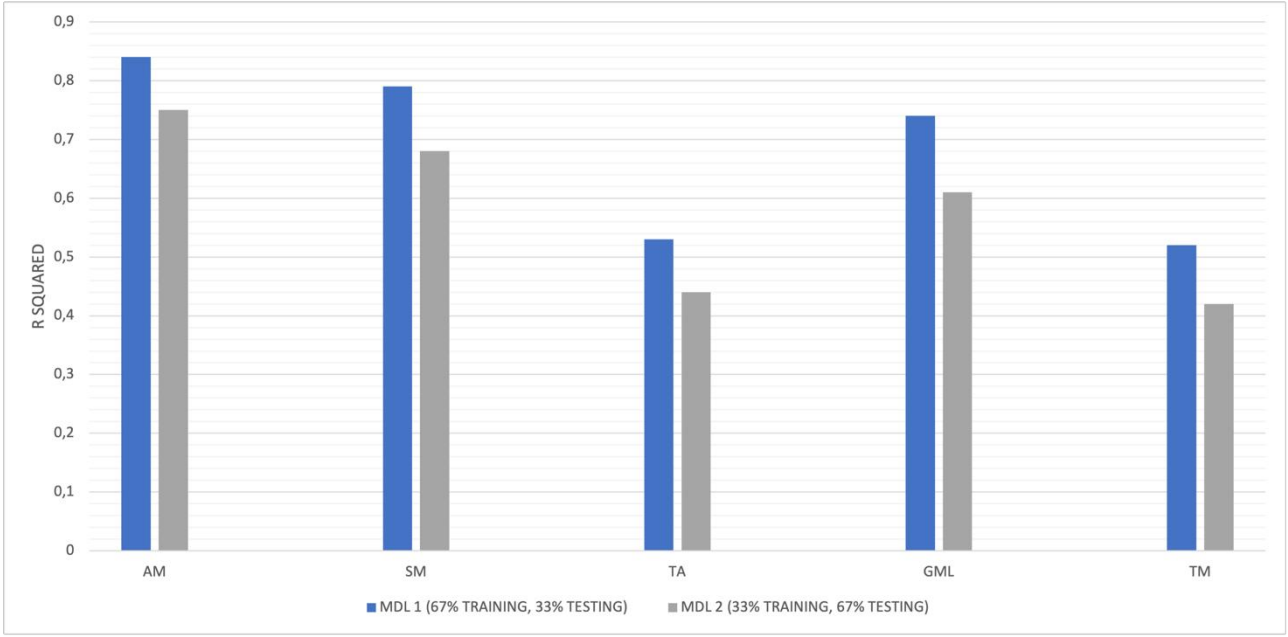

Figure 33: Histogram of R^2 obtained for the ankle joint. R-Squared obtained from the ankle angle regression considering all the six muscles reaches values around 0.80 for both Model 1 and Model 2; reducing the number of muscles from the initial configuration, R-Squared is diminished, with lower values from the configuration with thigh muscles (around 0.50).

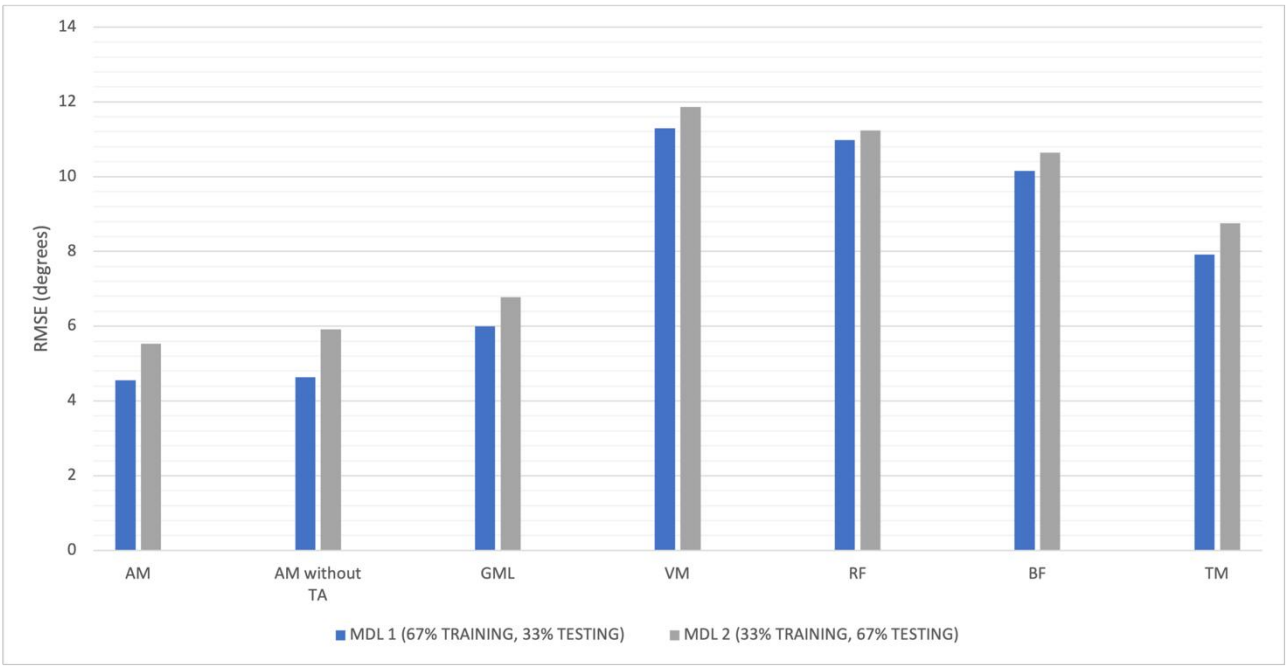

Figure 34: Histogram of RMSE obtained for the knee joint. To regress the knee angle, best results are achieved both from the configuration with all the six muscles and from the configuration with all the muscles excluding tibialis anterior (4°<RMSE<6°). Worst results are obtained considering the muscles that cross the knee joint alone. Choosing thigh muscles, RMSE is obtained with values higher than 6° and around 8°.

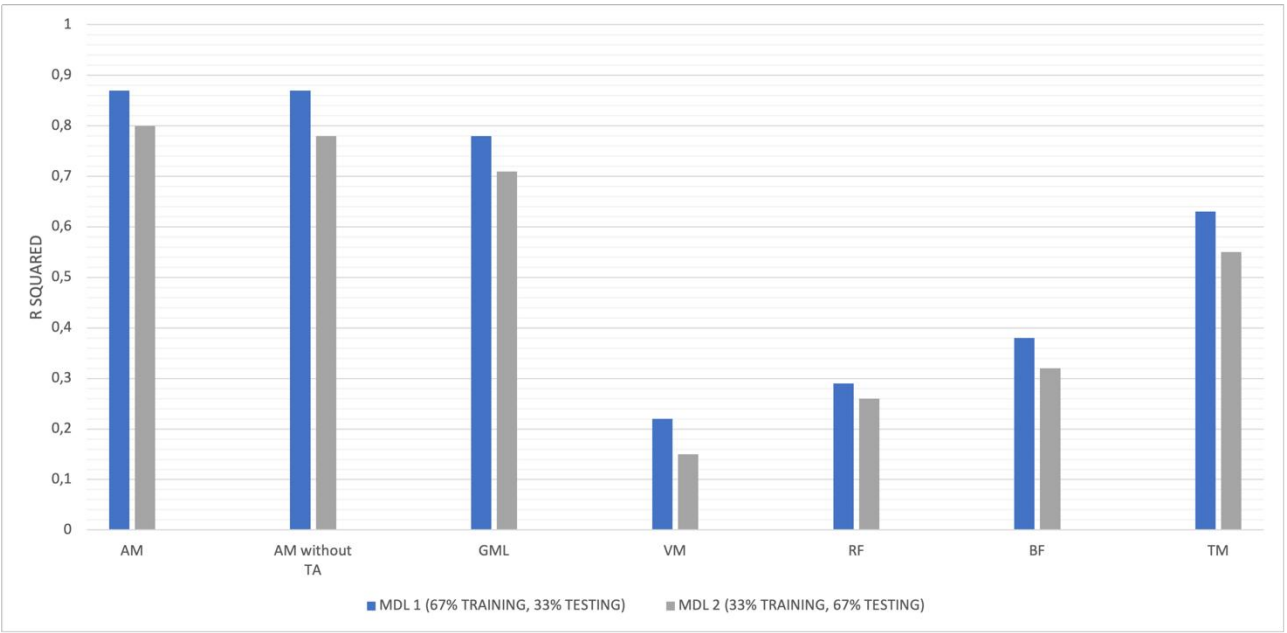

Figure 35: Histogram of R^2 obtained for the knee joint. Results obtained considering all the six muscles are the best with R-Squared between 0.80 and 0.90. Considering thigh muscles alone for the knee angle regression, R-Squared is low, with values around 0.60 both for Model 1 and Model 2.

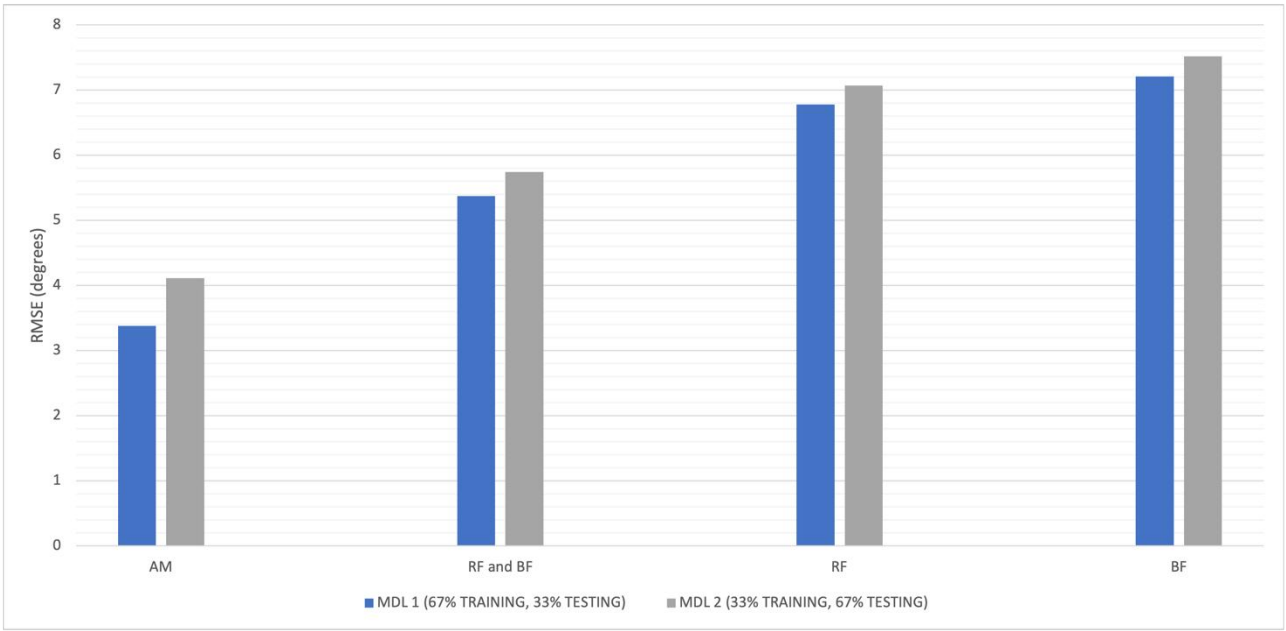

Figure 36: Histogram of RMSE obtained for the hip joint. Best results are achieved considering all the six muscles from the initial configuration with RMSE that reaches values around 4° for both Model 1 and Model 2. Regression performance is diminished considering RF and BF together and alone (5°<RMSE<8°).

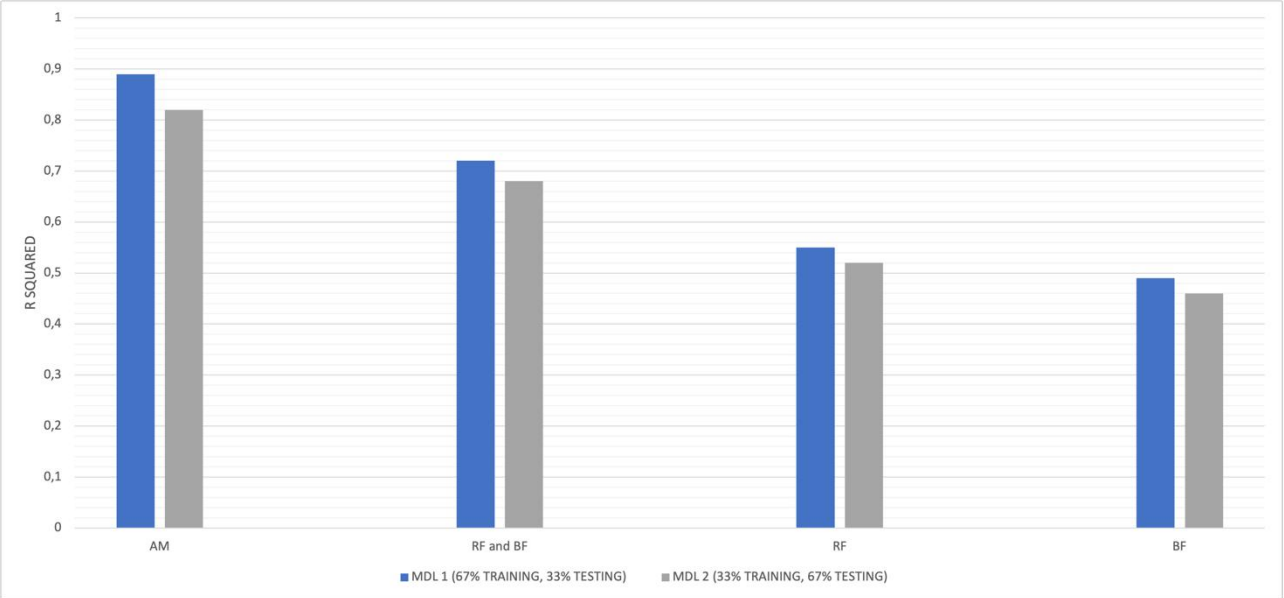

Figure 37: Histogram of R^2 obtained for the hip joint. R-Squared reaches value of 0.90 if the initial configuration with all the six muscles is considered for the hip angle regression. Worst results are obtained if only the muscles that cross the hip joint are considered: in fact, the R-Squared remains lower than 0.70 (considering RF and BF together), to reach values lower than 0.50 (considering BF muscle alone).

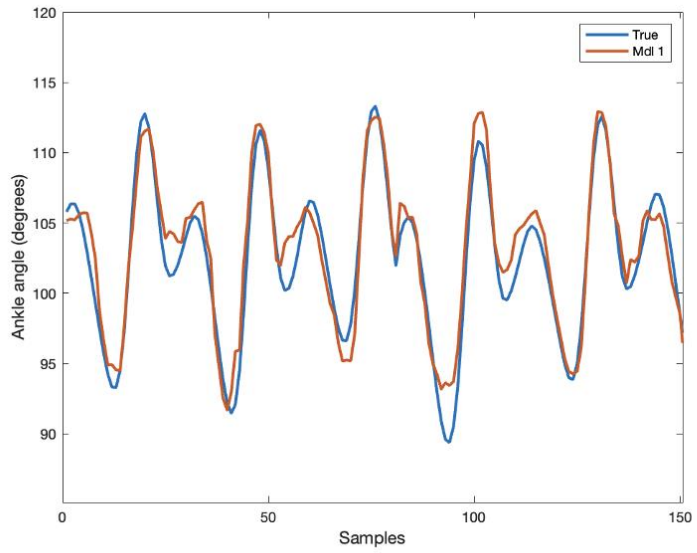

a)

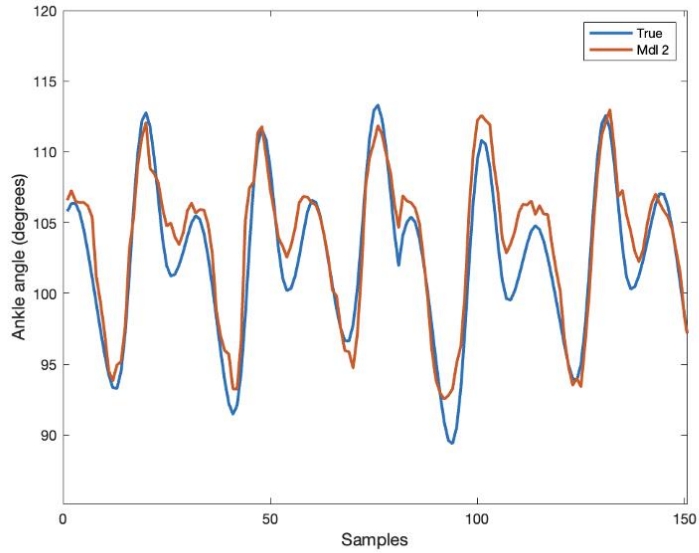

b)

Figure 38: The estimated angle and true angle of the ankle using Neural Networks regression Model 1 (a) and Model 2 (b) for the inter-trial analysis, considering all the six muscles.

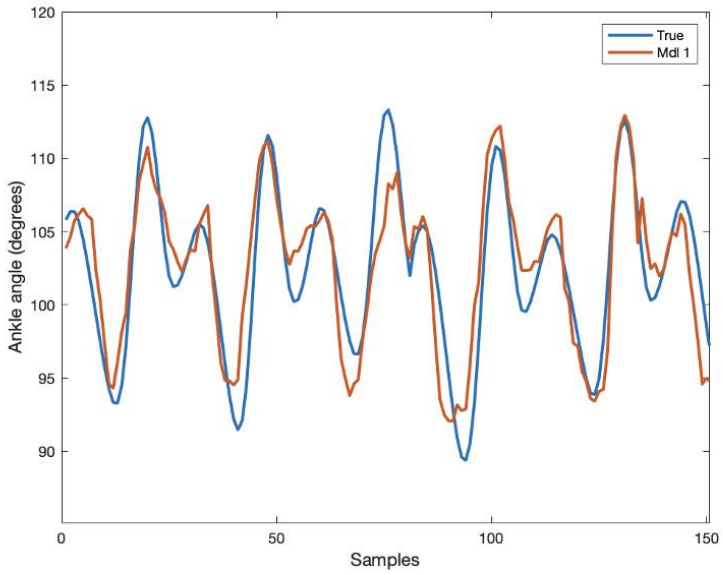

a)

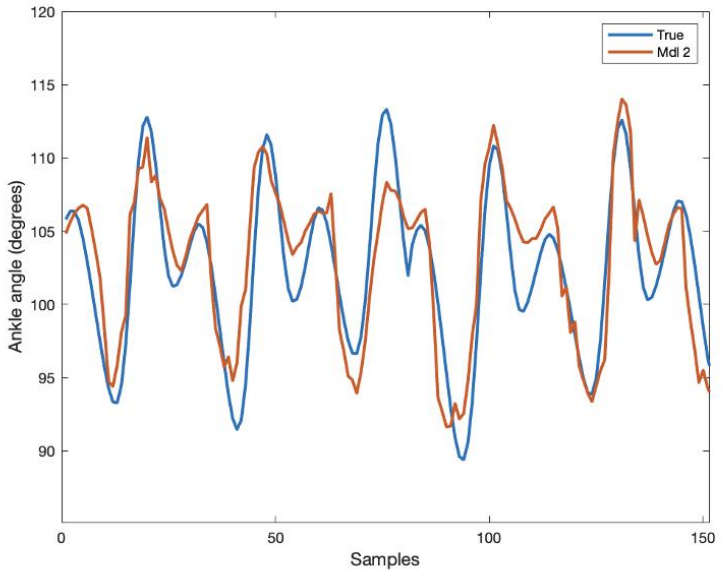

b)

Figure 39: The estimated angle and true angle of the ankle using Neural Networks regression Model 1 (a) and Model 2 (b) for the inter-trial analysis, considering the muscles of the thigh.

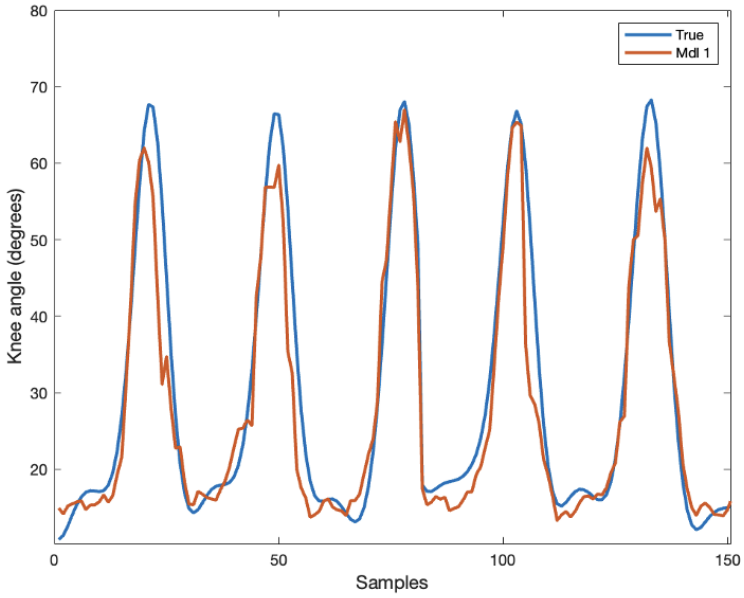

a)

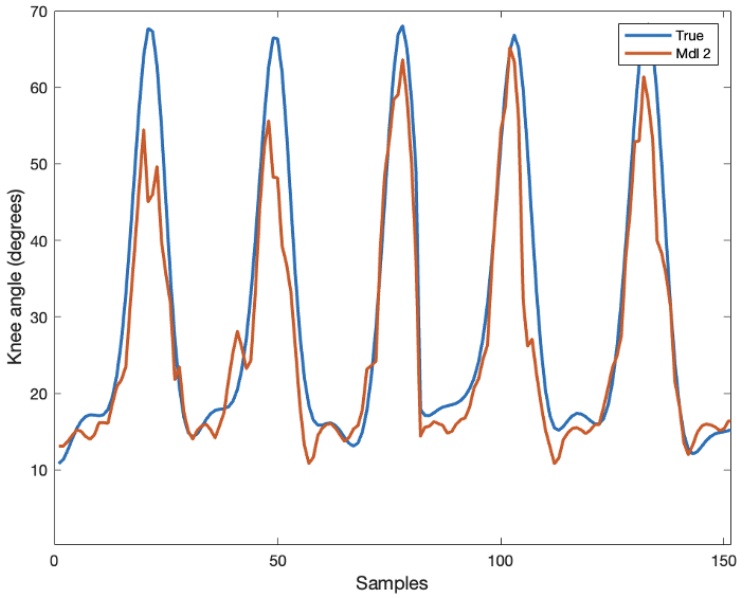

b)

Figure 40: The estimated angle and true angle of the knee using Neural Networks regression Model 1 (a) and Model 2 (b) for the inter-trial analysis, considering all the six muscles.

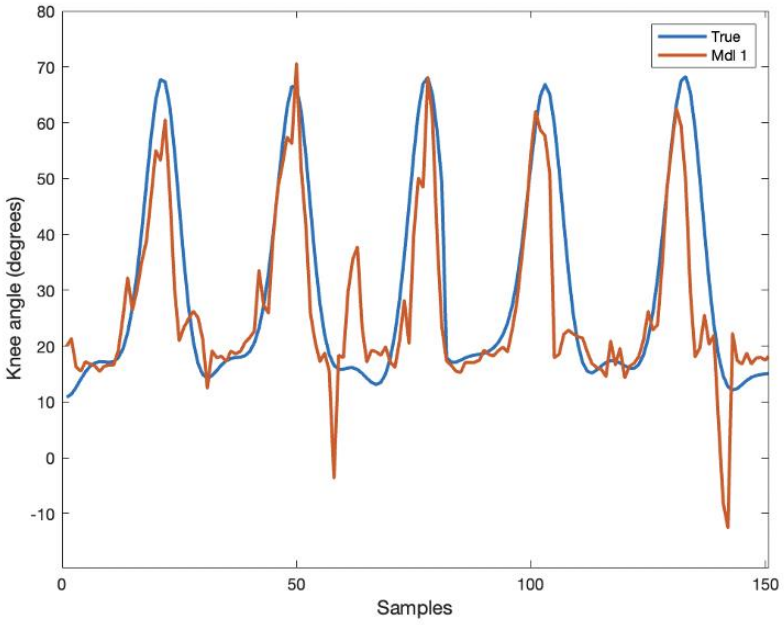

a)

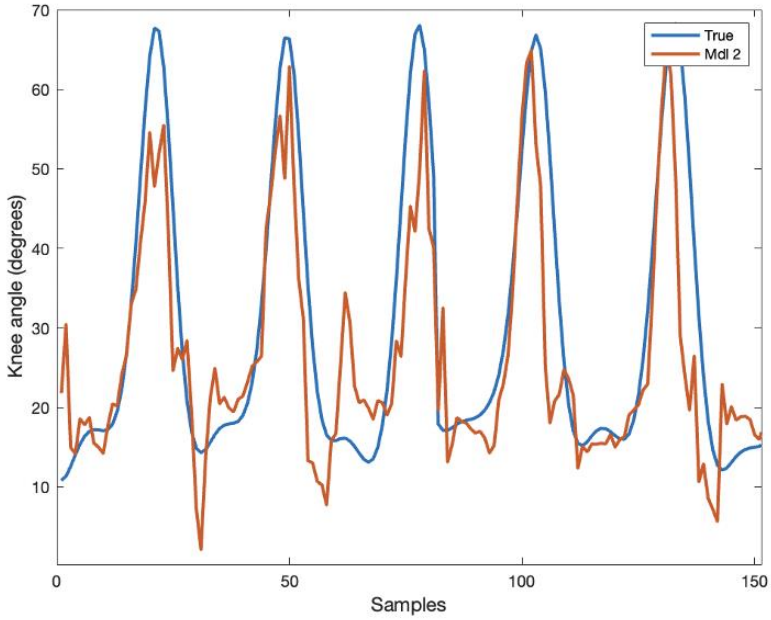

b)

Figure 41: The estimated angle and true angle of the knee using Neural Networks regression Model 1 (a) and Model 2 (b) for the inter-trial analysis, considering the muscles of the thigh.

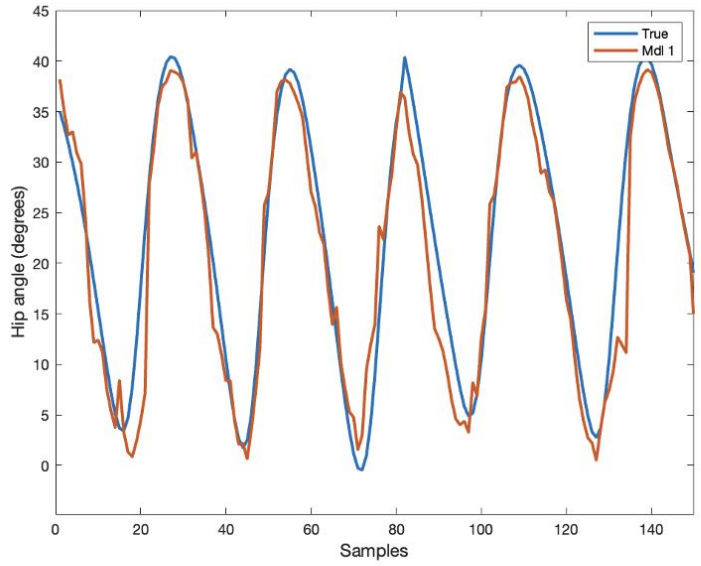

a)

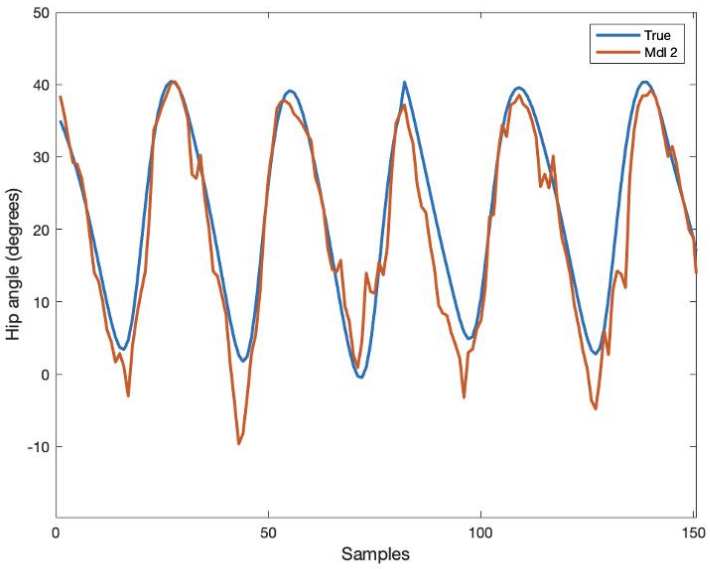

b)

Figure 42: The estimated angle and true angle of the hip using Neural Networks regression Model 1 (a) and Model 2 (b) for the inter-trial analysis, considering all the six muscles.

Moreover, additional analysis is done re-testing Model 1 and Model 2 on the same training data sets. Table 12, 13 and 14 show the results obtained.

ANKLE	***AM***		***SM***		***TA***		***GML***		***TM***	
	RMSE	R^2	*RMSE*	R^2	*RMSE*	R^2	*RMSE*	R^2	*RMSE*	R^2
MDL 1	2.38±0.39	0.89±0.04	3.08±0.44	0.82±0.10	4.78±0.58	0.56±0.10	3.42±0.57	0.77±0.08	4.39±1.00	0.62±0.20
MDL 2	2.16±0.83	0.91±0.02	2.97±1.01	0.83±0.09	4.82±0.82	0.55±0.20	3.28±1.11	0.79±0.14	4.13±1.12	0.66±0.27

Table 12: Mean and standard deviation of RMSE and R^2 metrics for training data.

KNEE	***AM***		***AM WITHOUT TA***		***GML***		***VM***		***RF***		***BF***		***TM***	
	RMSE	R^2	*RMSE*	R^2	*RMSE*	R^2	*RMSE*	R^2	*RMSE*	R^2	*RMSE*	R^2	*RMSE*	R^2
MDL 1	3,56± 1.24	0.92± 0.03	3.82± 1.20	0.91± 0.02	5.56± 1.27	0.80± 0.07	10.83± 2.26	0.28± 0.20	10.38± 2.74	0.36± 0.15	9.62± 2.42	0.44± 0.16	6.94± 2.21	0.71± 0.10
MDL 2	2.92± 1.83	0.95± 0.02	3.31± 1.96	0.93± 0.02	5.23± 1.36	0.83± 0.09	10.25± 2.54	0.34± 0.35	9.94± 2.89	0.40± 0.26	9.09± 2.48	0.49± 0.23	6.31± 2.55	0.76± 0.09

Table 13: Mean and standard deviation of RMSE and R^2 metrics for training data.

HIP	***AM***		***RF AND BF***		***RF***		***BF***	
	RMSE	R^2	*RMSE*	R^2	*RMSE*	R^2	*RMSE*	R^2
MDL 1	2.64±1.03	0.93±0.02	4.94±1.57	0.77±0.10	6.65±2.26	0.58±0.18	6.86±2.28	0.55±0.15
MDL 2	2.31±1.45	0.95±0.01	4.73±1.40	0.79±0.09	6.63±2.31	0.58±0.19	6.59±2.23	0.59±0.14

Table 14: Mean and standard deviation of RMSE and R^2 metrics for training data.

4 DISCUSSION AND CONCLUSION

In this section, results obtained from the two analyses are discussed starting from the effect on the estimation of joints angles due to the reduction of muscles from the initial configuration with six muscles, then these effects are explained considering more trials done by the subjects for the regression (inter-trial analysis). Further explanations on the statistical differences between the considered models for this study is reported.

4.1 Regression analysis reducing electrode's setup

Lower limbs joint angles have been estimated, in this study, through NN models from EMG signals. For each joint, regression was performed considering all electrodes setup (six electrodes on the right leg) and then performing the regression reducing electrode's setup, differently for each joint. Then, the effect of the electrodes setup on regression performance has been taken into account. This can be particularly relevant when data obtained by trans-tibial amputees are considered and when data by the only thigh muscles can be considered for the myoelectric control of ankle and knee prosthesis. Finally, regression was done with six neural networks models, starting from a model with large amount of training data (90%) with respect to testing data (10%), to finally consider models with lower amount of data for training and consequently higher number for testing. The results showed in Table 3, 4 and 5 explain that better results are achieved considering all the six muscles (for ankle: RMSE of 2.55 degrees and R^2 of 0.87 with Model 1; for knee: RMSE of 4.36 degrees and R^2 of 0.90 with Model 2; for hip: RMSE of 3.25 degrees and R^2 of 0.91 for Model 1), confirming in this way the reliability and robustness of the feed-forward NN models. For what concern the inter-trial analysis, good results are achieved as well with respect to the previous analysis done on each trial separately (Tables 9, 10 and 11). This means that, in order to obtain an estimation of the joint angles exploiting regressive methods, it could be sufficient non-complex architecture, as the feed-forward NN regression method used in this study (Figure 20). With the inter-trial analysis, it can be confirmed the robustness of data and the subdivision of data sets because the feed-forward NN models can give good performance in the joints angles regression with longer training and testing data and these results are similar to those obtained from the analysis performed on each trial. In fact, it has been seen that even one or more trials with a great amount of cycle times - about 70 steps on one trial and 150 steps on two trials - carried out by the same subject can be used as a training/testing set. This gives the possibility to achieve reliable results if one considers only six muscles in the overall electrodes' setup, while other studies considered instead more muscles in the electrodes' configuration [14], [16], [17],

[72]. For example, in the study of Chen et Al. [16] better results were achieved, considering ten muscles (biceps femoris, semitendinosus, vastus medialis, vastus lateralis, rectus femoris, sartorius, gastrocnemius medialis, gastrocnemius lateralis, tibialis anterior and soleus) in the surface EMG electrodes' setup and using Back Propagation (BP) Neural Network for the ankle, knee and hip angles regression and Deep Belief Neural Network for the extraction of the optimal features vectors, for what concern the R^2 (for the hip: achieved value of 0.96; for the knee: 0.97; for the ankle: 0.95). In a view of limitation of the EMG information, by considering different muscles configurations as explained in Section 2.7 (see Table 2), we have seen in our study that the performance of the models is considerably reduced with respect to the initial configuration with all muscles, as one could expect. A better view of this concept can be seen in the histograms of RMSE and R^2 in Figures 21, - 26 and for inter-trial analysis in Figures 32, - 37. RMSE when each muscle is considered alone or when a group of muscles (Shank Muscles-SM, Thigh Muscles-TM, Gastrocnemius Medialis and Lateralis-GML, Rectus Femoris-RF and Biceps Femoris-BF) with respect to a configuration with All Muscles (AM), is generally increased. However, some positive aspects in muscle reduction can be observed. Generally, regression analysis could be done in an optic of exploiting prosthesis for trans-amputees' subjects, as seen in some studies [20], [21]. For this reason, we had considered alone Thigh Muscles (TM) to do the regression of ankle and knee and evaluate the performance of this choice, but, as it can be seen in Tables 3, 4, 9 and 10, the regressor performance of R^2 for all the considered models is relatively low compared to all electrodes set up (but with a RMSE that remains still low for the ankle, even lower than 6°). Then, the considered TM group of muscles (Vastus Medialis, Rectus Femoris and Biceps Femoris) could not be sufficient to have a good regression performance on knee angle, given the high RMSE (lower value 8.63 for each trial, and lower value 7.92 for inter-trial regression). An additional aspect considered in this study is the role of shank muscles for ankle joint motion reconstruction. As it can be seen in Tables 3 and 9, the results obtained for RMSE and R^2 can show comparable performance when signals from all the electrodes are used (Figures 21, 22 and 32, 33). This means that, in order to do the regression of ankle angles, it could be just sufficient to consider the proximal muscles of the shank (Tibialis Anterior and Gastrocnemius Medialis and Lateralis), avoiding for instance the distal ones. For the regression of the knee angle, Tibialis Anterior resulted useless: in fact, it can be observed in Tables 4 and 10 and in Figures 23, 24, 34 and 35 that the RMSE and R^2 results are almost comparable to the case in which one considers all the six muscles in the complete electrodes configuration.

4.2 Regression models performance

Six models have been considered for the regression of ankle, knee, and hip angles on each trial for every muscle or group of muscles considered, and two models for the inter-trial regression for each group of muscles as well. To evaluate the statistical difference between the models, the Wilcoxon rank sum test was adopted on R^2 metrics. It was chosen R^2 to evaluate the statistical differences between the models because, unlike RMSE, R^2 is not sensitive to systematic errors and gives an overall sense on how well the model is good in predicting data [73]. Among the models reported in Tables 3, 4 and 5 for the regression on each trial, we evaluated the statistical difference between Model 1 and Model 6 because the differences in the amount of training and testing data between them were more respect to the other models and we wanted to verify possible statistical differences due to data subdivision between training and testing. Results of the statistical analysis performed between Model 1 and Model 6 revealed significant differences only for the hip joint when all muscles are considered (which gave a p-value<0.05) as we can see in Table 5.
In Tables 9, 10 and 11 it can be observed that there is a difference in R^2 between Model 1 and Model 2 that is statistically significant: it is between the models used to regress the ankle angle considering all the electrodes set up (Table 9). This explains the fact that all the models that showed not statistically differences in the R^2 metric are valid in the regression of the joint angles, so that a model with lower amount of training data could be as robust and reliable as a model with larger amount of training data with respect to testing data.

In conclusion it can be said that all the models used for the regression have demonstrated to be reliable and robust in the estimation of ankle, knee, and hip angles, with statistically differences between Model 1 and 6 for the estimation of the hip in the regression on each trial and between Model 1 and 2 for the estimation of the ankle in the inter-trial analysis.
It has been showed that good results are achieved considering all the electrodes' setup, comparable to the study of Xiong et Al. [14]. In the study of [14], in fact, better results are achieved, in terms of RMSE metric, for the ankle with respect to the knee. In the case of trans-amputee subjects, the estimation of joint angle for the use of transtibial prosthesis is very important. The models of Neural Network regression showed an RMSE for the ankle lower than 6°, choosing only the electrodes of the thigh for the regression. In this way, it showed that the use of a simple NN regression approach, to continuously predict joint kinematics using natural residual muscle activity, provides opportunities for direct (transparent) control of a prosthetic joint by the user. On the other hand, in our work, the models showed a R^2 value quite low (for ankle: the highest value among all the models is 0.56; for

knee: the highest value among the proposed models is 0.63), saying that the models could be not good enough in predicting the joint angle in case of transtibial amputees' subjects. In this study, in fact, better results are achieved considering more proximal muscles to the ankle (the muscles of the shank) giving the possibility to reduce the electrodes set up from 6 to only 3 electrodes in the estimation of ankle angle. For the knee, only muscles crossing the knee joint could be useful, excluding Tibialis Anterior. For the hip joint, only the complete set up has proved to be the most effective in the estimation of the joint angle. Further improvements of this study could be done. Firstly, more participants could take part to the experiments, and many other tasks could be involved (stair ascend, stair descend, walking at different speeds, etc.) to prove the efficacy of the method proposed in this study and to see if the neural network model is efficient; then, to improve the limitations done by the choice of using only one features set in time domain, the features set could be enlarged and, as in the study of Chen et Al. [16], it could be proposed a method of feature dimensionality reduction in order to reduce the time needed by the system to get the best model in a short time. In fact, in the study [16] it was employed a Deep Belief Network method by which the multi-channel surface EMG signals were encoded in low dimensional space and the optimal features were extracted. Another option could be to consider multiple time domain features combined together to compensate the limited information problem of one feature set while keeping the computation complexity relatively lower, as in the study done by Xiong et Al. [14]. Lastly, more muscles in the electrodes set up could be involved and if more channels in the surface EMG signal are used as input, the regression accuracy could be improved.

REFERENCES

[1] Tasch U.; *et al.*, "Volume 2: Automotive Systems; Bioengineering and Biomedical Technology," *Computational Mechanics; Controls; Dynamical Systems*, pp. 45–49, 2008.

[2] Cappello A., Cappozzo A., and di Prampero P. E., *Bioingegneria della postura e del movimento.* . 2003.

[3] Root M.L., Orien W.P., Wedd J.H., and Hughes R.J., "Biomechanical examination of the foot. ," *Clinical Biomechanics Corporation*, 1971.

[4] Loudon J and et Al., "The clinical orthopedic assessment guide: 2nd ed. ," *Kansas: Human Kinetics*, pp. 395–408, 2008.

[5] Davis III R.B., Ounpuu S., Tyburski D., and Gage J.R., "A gait analysis data collection and reduction technique. ," *Human Movement Science* , pp. 575–587, 1991.

[6] Levine D.F., Richards J., and Whittle M., "Whittle's Gait Analysis," *Elsevier Health Sciences*, 2012.

[7] Kim J.J., Lee M.H., and et Al., "Comparison of the maximum EMG levels recorded in maximum effort isometric contractions at five different knee flexion angles," *Korean Scoity Sport Biomech*, vol. 15, pp. 197–206, 2005.

[8] Yang J., Lee J., Lee B., and et Al., "The effects of elbow joint angle changes on elbow flexor and extensor muscle strength and activation," *J Phys Ther Sci*, vol. 26, pp. 1079–1082, 2014.

[9] Ha M. and Han D., "The relationship between knee joint angle and knee flexor and extensor muscle strength," *J Phys Ther Sci*, pp. 662–664, Apr. 2017.

[10] K. G. Rabe and N. P. Fey, "Evaluating Electromyography and Sonomyography Sensor Fusion to Estimate Lower-Limb Kinematics Using Gaussian Process Regression," *Front Robot AI*, vol. 9, Mar. 2022, doi: 10.3389/frobt.2022.716545.

[11] S. Au, M. Berniker, and H. Herr, "Powered ankle-foot prosthesis to assist level-ground and stair-descent gaits," *Neural Networks*, vol. 21, no. 4, pp. 654–666, May 2008, doi: 10.1016/j.neunet.2008.03.006.

[12] K. H. Ha, H. A. Varol, and M. Goldfarb, "Volitional control of a prosthetic knee using surface electromyography," *IEEE Trans Biomed Eng*, vol. 58, no. 1, pp. 144–151, Jan. 2011, doi: 10.1109/TBME.2010.2070840.

[13] J. A. Spanias, A. M. Simon, S. B. Finucane, E. J. Perreault, and L. J. Hargrove, "Online adaptive neural control of a robotic lower limb prosthesis," *J Neural Eng*, vol. 15, no. 1, p. 16015, Jan. 2018, doi: 10.1088/1741-2552/aa92a8.

[14] Dezhen Xiong, Daohui Zhang, Xingang Zhao, and Yiwen Zhao, *Continuous human gait tracking using sEMG signals*. 42nd Annual International Conference of the IEEE Engineering in Medicine & Biology Society (EMBC), 2020.

[15] E. v. Zabre-Gonzalez, L. Riem, P. A. Voglewede, B. Silver-Thorn, S. R. Koehler-McNicholas, and S. A. Beardsley, "Continuous Myoelectric Prediction of Future Ankle Angle and Moment Across Ambulation Conditions and Their Transitions," *Front Neurosci*, vol. 15, Aug. 2021, doi: 10.3389/fnins.2021.709422.

[16] J. Chen, X. Zhang, Y. Cheng, and N. Xi, "Surface EMG based continuous estimation of human lower limb joint angles by using deep belief networks," *Biomed Signal Process Control*, vol. 40, pp. 335–342, Feb. 2018, doi: 10.1016/j.bspc.2017.10.002.

[17] Q. L. Li, Y. Song, and Z. G. Hou, "Estimation of Lower Limb Periodic Motions from sEMG Using Least Squares Support Vector Regression," *Neural Process Lett*, vol. 41, no. 3, pp. 371–388, Jun. 2015, doi: 10.1007/s11063-014-9391-4.

[18] T. Prasertsakul, J. Poonsiri, and W. Charoensuk, "Prediction gait during ascending stair by using Artificial Neural Networks," 2012. doi: 10.1109/BMEiCon.2012.6465464.

[19] S. Dey, S. Boughorbel, and A. F. Schilling, "Learning a Shared Model for Motorized Prosthetic Joints to Predict Ankle-Joint Motion," Nov. 2021, [Online]. Available: http://arxiv.org/abs/2111.07419

[20] S. Farmer, B. Silver-Thorn, P. Voglewede, and S. A. Beardsley, "Within-socket myoelectric prediction of continuous ankle kinematics for control of a powered transtibial prosthesis," *J Neural Eng*, vol. 11, no. 5, p. 56027, Sep. 2014, doi: 10.1088/1741-2560/11/5/056027.

[21] B. Silver-Thorn, T. Current, and B. Kuhse, "Preliminary investigation of residual limb plantarflexion and dorsiflexion muscle activity during treadmill walking for trans-tibial amputees," *Prosthet Orthot Int*, vol. 36, no. 4, 2012, [Online]. Available: https://journals.lww.com/poijournal/Fulltext/2012/36040/Preliminary_investigation_of_residual_limb.5.aspx

[22] H. Huang, F. Zhang, L. J. Hargrove, Z. Dou, D. R. Rogers, and K. B. Englehart, "Continuous locomotion-mode identification for prosthetic legs based on neuromuscular - Mechanical fusion," *IEEE Trans Biomed Eng*, vol. 58, no. 10 PART 1, pp. 2867–2875, Oct. 2011, doi: 10.1109/TBME.2011.2161671.

[23] S. Dey, T. Yoshida, M. Ernst, T. Schmalz, and A. F. Schilling, "A random forest approach for continuous prediction of joint angles and moments during walking: An implication for controlling active knee-ankle prostheses/orthoses," in *2019 IEEE International Conference on*

Cyborg and Bionic Systems, CBS 2019, Sep. 2019, pp. 66–71. doi: 10.1109/CBS46900.2019.9114439.

[24] S. Dey, T. Yoshida, and A. F. Schilling, "Feasibility of Training a Random Forest Model With Incomplete User-Specific Data for Devising a Control Strategy for Active Biomimetic Ankle," *Front Bioeng Biotechnol*, vol. 8, Aug. 2020, doi: 10.3389/fbioe.2020.00855.

[25] Sutherland D.H., Kaufman K.R., and Moitoza J.R., "Kinematic of normal human walking," *Human Walking*, pp. 23–44, 1994.

[26] Kaufman K., "Future directions in gait analysis," *Gait Analysis in the Science of Rehabilitation*, 1998.

[27] Kalita, Bhaben & Narayan, Jyotindra & Dwivedy, and Santosha, "Development of Active Lower Limb Robotic-Based Orthosis and Exoskeleton Devices: A Systematic Review," *Int J Soc Robot*, 2021.

[28] J. Vrints, E. Koninckx, M. van Leemputte, and I. Jonkers, "The effect of saddle position on maximal power output and moment generating capacity of lower limb muscles during isokinetic cycling," *J Appl Biomech*, vol. 27, no. 1, pp. 1–7, 2011, doi: 10.1123/jab.27.1.1.

[29] M. Porta *et al.*, "Lower limb kinematics in individuals with hip osteoarthritis during gait: A focus on adaptative strategies and interlimb symmetry," *Bioengineering*, vol. 8, no. 4, 2021, doi: 10.3390/bioengineering8040047.

[30] A. Ferrari *et al.*, "Quantitative comparison of five current protocols in gait analysis," *Gait Posture*, vol. 28, no. 2, pp. 207–216, Aug. 2008, doi: 10.1016/j.gaitpost.2007.11.009.

[31] Y. Kim, S. Hwang, S. Myeong, Y. Keum, H. Kim, and S. Myung, "The evaluation of the lower extremity joint's contribution for the support moment in unexpected step-down walking," 2005. [Online]. Available: https://www.researchgate.net/publication/301221843

[32] Balboni G.C., Bastianini A., and et Al., *Anatomia Umana*, vol. 1. 1993.

[33] A. Santuz *et al.*, "Modular control of human movement during running: An open access data set," *Front Physiol*, vol. 9, no. OCT, Oct. 2018, doi: 10.3389/fphys.2018.01509.

[34] F. Lacquaniti, Y. P. Ivanenko, and M. Zago, "Patterned control of human locomotion," *Journal of Physiology*, vol. 590, no. 10. pp. 2189–2199, May 2012. doi: 10.1113/jphysiol.2011.215137.

[35] Keith L. and et Al., *Clinically oriented anatomy*. Philadelphia, 2018.

[36] M. Paoletti, A. Belli, L. Palma, M. Vallasciani, and P. Pierleoni, "A Wireless Body Sensor Network for Clinical Assessment of the Flexion-Relaxation Phenomenon," *Electronics (Basel)*, vol. 9, no. 6, p. 1044, Jun. 2020, doi: 10.3390/electronics9061044.

[37] M. Zahak, "Signal Acquisition Using Surface EMG and Circuit Design Considerations for Robotic Prosthesis," in *Computational Intelligence in Electromyography Analysis - A*

Perspective on Current Applications and Future Challenges, InTech, 2012. doi: 10.5772/52556.

[38] S. L. Pullman, D. S. Goodin, A. I. Marquinez, S. Tabbal, and M. Rubin, "Clinical utility of surface EMG [RETIRED]," *Neurology*, vol. 55, no. 2, pp. 171–177, Jul. 2000, doi: 10.1212/WNL.55.2.171.

[39] A. Tatarelli *et al.*, "Global muscle coactivation of the sound limb in gait of people with transfemoral and transtibial amputation," *Sensors (Switzerland)*, vol. 20, no. 9, May 2020, doi: 10.3390/s20092543.

[40] L. McManus, G. de Vito, and M. M. Lowery, "Analysis and Biophysics of Surface EMG for Physiotherapists and Kinesiologists: Toward a Common Language With Rehabilitation Engineers," *Front Neurol*, vol. 11, Oct. 2020, doi: 10.3389/fneur.2020.576729.

[41] M. Asghari Oskoei and H. Hu, "Myoelectric control systems-A survey," *Biomedical Signal Processing and Control*, vol. 2, no. 4. Elsevier BV, pp. 275–294, 2007. doi: 10.1016/j.bspc.2007.07.009.

[42] M. Zecca, S. Micera, M. C. Carrozza, and P. Dario, "Control of Multifunctional Prosthetic Hands by Processing the Electromyographic Signal," *Crit Rev Biomed Eng*, vol. 30, no. 4–6, pp. 459–485, 2002, doi: 10.1615/CritRevBiomedEng.v30.i456.80.

[43] A. Phinyomark, C. Limsakul, and P. Phukpattaranont, "EMG feature extraction for tolerance of 50 Hz interference," 2009. [Online]. Available: http://icet2009.ftn.ns.ac.yu

[44] A. Phinyomark, P. Phukpattaranont, and C. Limsakul, "Feature reduction and selection for EMG signal classification," *Expert Syst Appl*, vol. 39, no. 8, pp. 7420–7431, Jun. 2012, doi: 10.1016/j.eswa.2012.01.102.

[45] L. S. Praveen, S. N. Nagananda, and P. Shankapal, "Design and Development of Real Time Bionic Hand Control Using EMG Signal," in *2018 IEEE International Conference on Electronics, Computing and Communication Technologies (CONECCT)*, Mar. 2018, pp. 1–4. doi: 10.1109/CONECCT.2018.8482393.

[46] M. Zecca, S. Micera, M. C. Carrozza, and P. Dario, "Control of Multifunctional Prosthetic Hands by Processing the Electromyographic Signal," *Crit Rev Biomed Eng*, vol. 45, no. 1–6, pp. 383–410, 2017, doi: 10.1615/CritRevBiomedEng.v45.i1-6.150.

[47] A. Ullah, S. Ali, I. Khan, M. A. Khan, and S. Faizullah, "Effect of analysis window and feature selection on classification of hand movements using EMG signal," in *Advances in Intelligent Systems and Computing*, 2021, vol. 1252 AISC, pp. 400–415. doi: 10.1007/978-3-030-55190-2_30.

[48] O. W. Samuel *et al.*, “Intelligent EMG pattern recognition control method for upper-limb multifunctional prostheses: Advances, current challenges, and future prospects,” *IEEE Access*, vol. 7, pp. 10150–10165, 2019, doi: 10.1109/ACCESS.2019.2891350.

[49] I. Kang, P. Kunapuli, and A. J. Young, “Real-Time Neural Network-Based Gait Phase Estimation Using a Robotic Hip Exoskeleton,” *IEEE Trans Med Robot Bionics*, vol. 2, no. 1, pp. 28–37, Feb. 2020, doi: 10.1109/TMRB.2019.2961749.

[50] S. J. Preece, J. Y. Goulermas, L. P. J. Kenney, and D. Howard, “A comparison of feature extraction methods for the classification of dynamic activities from accelerometer data,” *IEEE Trans Biomed Eng*, vol. 56, no. 3, pp. 871–879, Mar. 2009, doi: 10.1109/TBME.2008.2006190.

[51] T. R. Farrell and R. F. Weir, “The optimal controller delay for myoelectric prostheses,” *IEEE Transactions on Neural Systems and Rehabilitation Engineering*, vol. 15, no. 1, pp. 111–118, Mar. 2007, doi: 10.1109/TNSRE.2007.891391.

[52] M. N. Nyan, F. E. H. Tay, K. H. W. Seah, and Y. Y. Sitoh, “Classification of gait patterns in the time-frequency domain,” *J Biomech*, vol. 39, no. 14, pp. 2647–2656, 2006, doi: 10.1016/j.jbiomech.2005.08.014.

[53] N. Wang, E. Ambikairajah, N. H. Lovell, S. Member, and B. G. Celler, “Accelerometry Based Classification of Walking Patterns Using Time-frequency Analysis,” 2007.

[54] S. I. Sabilla and R. Sarno, “Development of wavelet transforms to predict methane in chili using the electronic nose,” in *2017 International Conference on Advanced Mechatronics, Intelligent Manufacture, and Industrial Automation (ICAMIMIA)*, 2017, pp. 271–276. doi: 10.1109/ICAMIMIA.2017.8387600.

[55] D. Singh and B. Singh, “Investigating the impact of data normalization on classification performance,” *Appl Soft Comput*, vol. 97, Dec. 2020, doi: 10.1016/j.asoc.2019.105524.

[56] J. J. Hopfield, “Neural networks and physical systems with emergent collective computational abilities.,” *Proceedings of the National Academy of Sciences*, vol. 79, no. 8, pp. 2554–2558, Apr. 1982, doi: 10.1073/pnas.79.8.2554.

[57] Srivignesh Rajan, “A Walk-through of Regression Analysis Using Artificial Neural Networks in Tensorflow,” *Data Science Blogathon*, Aug. 2021.

[58] P. L. Fernández-Cabán, F. J. Masters, and B. M. Phillips, “Predicting roof pressures on a low-rise structure from freestream turbulence using artificial neural networks,” *Front Built Environ*, vol. 4, Nov. 2018, doi: 10.3389/fbuil.2018.00068.

[59] S. Wieczorek, D. Filipiak, and A. Filipowska, “Semantic Image-Based Profiling of Users’ Interests with Neural Networks.”

[60] M. Minsky and S. A. Papert, *Perceptrons*. The MIT Press, 2017. doi: 10.7551/mitpress/11301.001.0001.

[61] J. Schmidhuber, "Deep learning in neural networks: An overview," *Neural Networks*, vol. 61, pp. 85–117, Jan. 2015, doi: 10.1016/j.neunet.2014.09.003.

[62] A. Zell, "Simulation neuronaler Netze," 1994.

[63] P. Auer, H. Burgsteiner, and W. Maass, "A learning rule for very simple universal approximators consisting of a single layer of perceptrons," *Neural Networks*, vol. 21, no. 5, pp. 786–795, Jun. 2008, doi: 10.1016/j.neunet.2007.12.036.

[64] P. Tahmasebi and A. Hezarkhani, "Application of a Modular Feedforward Neural Network for Grade Estimation," *Natural Resources Research*, vol. 20, no. 1, pp. 25–32, Mar. 2011, doi: 10.1007/s11053-011-9135-3.

[65] X. Glorot and Y. Bengio, "Understanding the difficulty of training deep feedforward neural networks." [Online]. Available: http://www.iro.umontreal.

[66] J. D. Gibbons and S. Chakraborti, "Nonparametric Statistical Inference," in *International Encyclopedia of Statistical Science*, Berlin, Heidelberg: Springer Berlin Heidelberg, 2011, pp. 977–979. doi: 10.1007/978-3-642-04898-2_420.

[67] M. Hollander, D. A. Wolfe, and E. Chicken, *Nonparametric Statistical Methods*. Wiley, 2015. doi: 10.1002/9781119196037.

[68] R. J. Hyndman and A. B. Koehler, "Another look at measures of forecast accuracy," *Int J Forecast*, vol. 22, no. 4, pp. 679–688, Oct. 2006, doi: 10.1016/j.ijforecast.2006.03.001.

[69] R. G. Pontius, O. Thontteh, and H. Chen, "Components of information for multiple resolution comparison between maps that share a real variable," *Environ Ecol Stat*, vol. 15, no. 2, pp. 111–142, Jun. 2008, doi: 10.1007/s10651-007-0043-y.

[70] C. J. Willmott and K. Matsuura, "On the use of dimensioned measures of error to evaluate the performance of spatial interpolators," *International Journal of Geographical Information Science*, vol. 20, no. 1, pp. 89–102, Jan. 2006, doi: 10.1080/13658810500286976.

[71] A. Colin Cameron and F. A. G. Windmeijer, "An R-squared measure of goodness of fit for some common nonlinear regression models," *J Econom*, vol. 77, no. 2, pp. 329–342, Apr. 1997, doi: 10.1016/S0304-4076(96)01818-0.

[72] C. Li, H. He, S. Yin, H. Deng, and Y. Zhu, "Continuous Angle Prediction of Lower Limb Knee Joint Based on sEMG," 2021. doi: 10.1109/RASSE53195.2021.9686816.

[73] Jason Brownlee, "Regression metrics for machine learning," *Python machine learning*, Jan. 2021.